Cholecystokinin modulates age-dependent Thalamocortical Neuroplasticity

Xiao Li[1,2,†,*], Jingyu Feng[1,3,†], Xiaohan Hu[1], Peipei Zhou[1], Tao Chen[1], Xuejiao Zheng[1,2], Peter Jendrichovsky[1], Xue Wang[1], Mengying Chen[1], Hao Li[1], Xi Chen[1,2], Dingxuan Zeng[1], Mengfan Zhang[1], Zhoujian Xiao[1], Ling He[1], Stephen Temitayo Bello[1], Jufang He[1,2,*]

Department of Neuroscience, City University of Hong Kong, Tat Chee Avenue, Kowloon, Hong Kong SAR, China

Affiliations

[1]Department of Neuroscience, City University of Hong Kong, Kowloon Tong, Hong Kong.

[2]City University of Hong Kong Shenzhen Research Institute, Shenzhen, China.

[3]Department of Neuroscience, University of Rochester Medical Center, New York, USA

[†]Equal Contributions

*Corresponding Author:

Xiao Li. Address: Department of Neuroscience, City University of Hong Kong, Kowloon Tong, Hong Kong. Email: xli293@cityu.edu.hk

Jufang He. Address: Department of Neuroscience, City University of Hong Kong, Kowloon Tong, Hong Kong. Tel: (825) 34427042. Email: jufanghe@cityu.edu.hk

Keywords

Auditory cortex, medial geniculate body, long-term potentiation, sound discrimination, prepulse inhibition of startle reflex, cholecystokinin

Abstract

The thalamocortical pathway exhibits neuroplasticity not only during the critical period but also in adulthood. Here, we aimed to investigate the modulation of age-dependent thalamocortical plasticity by cholecystokinin (CCK). Our findings revealed the expression of CCK in thalamocortical neurons, and high-frequency stimulation (HFS) of the thalamocortical pathway elicited the release of CCK in auditory cortex (ACx), as evidenced by CCK sensor. HFS of the medial geniculate body (MGB) induced thalamocortical long-term potentiation (LTP) in wildtype young adult mice. However, knockdown of Cck expression in MGB neurons or blockade of the CCK-B receptor (CCKBR) in ACx effectively abolished HFS-induced LTP. Notably, this LTP could not be elicited in both juvenile mice (week 3) and mice over 18 months old, due to the absence of CCKBR in juvenile mice and the inability of CCK to be released in aged mice. Remarkably, the administration of exogenous CCK into the auditory cortex of the aged mice restored this LTP, accompanied by a significant improvement in frequency discrimination. These findings suggest the potential of CCK as a therapeutic intervention for addressing neurodegenerative deficits associated with thalamocortical neuroplasticity.

Introduction

Long-term potentiation (LTP) in the thalamocortical pathway plays a crucial role in the establishment and refinement of the topographical map in sensory cortices during development. In the somatosensory system, thalamocortical LTP can be induced by pairing the pre- and postsynaptic activation within the first postnatal week *in vitro* [1]. Disruption of NMDA receptor function has been shown to impede the formation of the topographical map of somatosensory cortex [2-4]. Exposure of neonatal mice to a tone presentation during early postnatal days significantly altered the tonotopic map in the auditory cortex (ACx) [5]. Towards the end of the critical period for topographical map formation in each sensory modality, neonatal LTP in the thalamocortical pathway vanished due to the developmental switch of NMDA receptor subunits, resulting in reduced susceptibility of sensory cortices to passive stimuli-induced modulations [6-8]. However, emerging evidence suggests that thalamocortical plasticity remains important for normal adult learning [9-12]. Sensory deprivation or sensory experience can reactivate the plasticity of thalamocortical input in adulthood [13-18]. In the adult auditory cortex, cortical map plasticity can be induced by pairing sound stimuli with activation of cholinergic inputs originating from the nucleus basalis[19]. High-frequency stimulation (HFS) applied to the dorsal lateral geniculate body (LGN) or medial geniculate body (MGB) in vivo can induce LTP in the sensory cortex of rats older than eight weeks [20-22]. This HFS-induced thalamocortical LTP has been demonstrated to account for perceptual learning in the post-critical period [23]. Nevertheless, the underlying mechanisms of thalamocortical plasticity in the mature brain remain elusive.

Previous studies have highlighted the crucial role of CCK, acting through its CCK-B receptor, in cortical plasticity [24,25]. The presence of CCK facilitates the potentiation of cortical

synaptic strength following presynaptic and postsynaptic neuronal activity [24]. Moreover, high-frequency stimulation (HFS) has been shown to induce cortical LTP in a manner that is dependent on CCK [25,26]. HFS of entorhino-neocortical pathway triggers CCK release from its terminals in the ACx, subsequently leading to cortico-cortical LTP and the formation of sound-sound associative memory [25,26], as well as visuoauditory associative memory [27,28]. Pharmacological blockade of CCKBR inhibits HFS-induced neocortical LTP and disrupts the formation of associative memory [24,25].

In the present study, we hypothesize that CCK, expressed in the MGB, plays an essential role in the formation of thalamocortical LTP in adult brain. We propose that the expression levels of CCK and its CCK-B receptor correlate with the emergence of thalamocortical LTP at distinct stages of postnatal development. To test this hypothesis, we investigated the existence of the HFS-induced thalamocortical LTP while specifically down-regulating Cck expression in MGB neurons or blocking CCKBR via its antagonist in the ACx. Furthermore, we utilized optogenetics to selectively activate the CCK-positive thalamocortical neurons for LTP induction. To assess CCK release from thalamocortical projections triggered by HFS, we employed a specialized CCK sensor. Additionally, we utilized RNAscope in situ hybridization and immunohistochemistry techniques to explore the relationship between thalamocortical LTP and the ontogeny of CCK and CCKBR expression at different life stages. In parallel, CCK release in aged mice was examined using the CCK sensor. Finally, we investigated whether exogenous application of CCK could rescue the thalamocortical LTP deficit in old animals and whether the restored thalamocortical neuroplasticity could improve sound discrimination in a behavioral experiment.

Results

HFS-induced thalamocortical LTP enhanced neuronal responses to a natural stimulus in the ACx.

In the present study, we initially applied HFS to the MGB in an *in-vivo* preparation to induce thalamocortical LTP and investigated its impact on cortical neuronal responses to the natural stimulus (sound) in adult mice. We placed stimulation electrodes in the MGB and recording electrodes in the ACx of 8-weeks old mice (Figure 1A). Both electrodes effectively captured neuronal responses to noise-bursts (Figure 1B). Field excitatory postsynaptic potential (fEPSP) in response to the electrical stimulation (ES) in the MGB was measured. Consistent with previous findings [21,22], HFS (Figure 1C) successfully induced thalamocortical LTP in the young adult mice (Figure 1D). The slope of fEPSPs, measured 1 h after the HFS, was potentiated by 30.0 ± 4.8% compared to the baseline before the HFS (Figure 1D, one-way RM ANOVA, $F[1,12] = 39.4$; pairwise comparison, before vs. after HFS, 100.7 ± 0.4% vs. 130.7 ± 4.8%, $p < 0.001$, n = 13 different recording and stimulation site, from N = 10 mice).

We subsequently examined whether the neuronal responses to the natural auditory stimulus in the ACx were also potentiated after the HFS-induced thalamocortical LTP (Figure 1E). As demonstrated in the example, the firing rate of the neuronal responses to the noise-burst stimulus in the ACx increased following HFS (Figure 1F). The fEPSPs of the neuronal responses to the noise burst stimulus also exhibited significant potentiation after HFS in the MGB (Figure 1G, one-way RM ANOVA, $F[1,16] = 67.0$; pairwise comparison, before vs. after HFS, 98.9 ± 1.7%

vs. 135.4 ± 2.9%, $p < 0.001$, $n = 17$, from 6 mice), indicating that recorded thalamocortical LTP facilitated neuronal responses in ACx to the natural stimulus. Notably, these experiments were conducted in the brains of adult mice, thereby confirming the presence of thalamocortical plasticity that can be induced by HFS in the auditory system of mice beyond the critical period.

HFS-induced thalamocortical LTP is CCK-dependent.

Previous studies have demonstrated that both exogenous and endogenous CCK can induce synaptic plasticity in different neural pathways [24-29]. HFS of entorhino-neocortical terminals triggers the release of CCK, thereby facilitating the formation of cortical LTP [25,26]. Moreover, CCK expression is abundant in MGB neurons [30-32], and high densities of CCK receptors are specifically located in layer IV of the auditory cortex[33], which is the main target of thalamocortical afferents. Based on these findings, we formulated the hypothesis that the HFS-induced thalamocortical LTP is also CCK-dependent.

To obtain direct evidence that HFS of the thalamocortical CCK projections induces homosynaptic LTP, we employed optogenetic manipulation of specific projection neurons. Cre-dependent AAV9-EFIa-DIO-ChETA-EYFP was injected into MGB of CCK-Cre mice. The EYFP labeling marked CCK-positive neurons in MGB, and the thalamocortical projection fibers mainly targeted layer IV of the ACx, as shown in Figure 2A upper panel. Immunochemistry staining further revealed colocalization of projection terminals from MGB CCK neurons with the majority of CCKBRs in ACx (Figure 2A lower panel). During optogenetic electrophysiology experiment, a glass recording electrode was inserted into layer IV of the ACx, and an optic fiber

was positioned near the recording electrode for laser activation of the thalamocortical terminals (Figure 2B upper left, and Figure S1A). Following a stable 16-min recording baseline of laser-evoked thalamocortical fEPSPs, high-frequency laser stimulation (HFLS) was delivered to the ACx. The fEPSPs evoked by HFLS demonstrated reliable synchronization of thalamocortical afferent activation with the 80 Hz laser stimulation (Figure S1B). Significantly, robust LTP was observed after HFLS (Figure 2B, one-way RM ANOVA, $F[1,24] = 62.8$; pairwise comparison, before vs. after HFLS-ACx, 100.2 ± 0.7% vs. 131.0 ± 3.8%, $p < 0.001$, $n = 25$ different recording and stimulation site, from 5 mice). Additionally, we performed HFLS of the MGB cell body instead of stimulating thalamocortical terminals. The fEPSPs elicited by the laser in MGB exhibited significant potentiation after HFLS (Figure S1C, one-way RM ANOVA, $F[1,17] = 31.8$; pairwise comparison, before vs. after HFLS-MGB, 99.6 ± 1.4% vs. 130.0 ± 4.7%, $p < 0.001$, $n = 18$, from 6 mice). These findings support the notion that HF activation of thalamocortical CCK projections enables thalamocortical LTP, potentially through the induction of homosynaptic CCK release.

To further substantiate the dependence of HFS-induced thalamocortical LTP on CCK, we specifically knocked down the Cck expression in the MGB by injecting AAV constructs carrying a short hairpin RNA (shRNA) targeting Cck (anti-Cck) or a nonsense sequence (anti-Scramble, Figure 2C). Successful down-regulation of Cck mRNA levels by anti-Cck shRNAs was confirmed in vivo [29]. No discernible differences were observed in the ACx responses to MGB stimulation between the animals that received the anti-CCK virus injection and those that were injected with the anti-scramble virus (as shown in Figure 2D upper middle). Notably, the anti-Cck group exhibited no induction of thalamocortical LTP following HFS, while the anti-

Scramble control group showed significant LTP (Figure 2D, two-way RM ANOVA, $F[1,31] = 50.3$, $p<0.001$, pairwise comparison: anti-Cck, before vs. after HFS, 99.7 ± 0.5% vs. 99.2 ± 2.9%, $p = 0.859$, n=16 from 10 mice; anti-Scramble, before vs. after HFS, 100.8 ± 0.5% vs. 129.4 ± 2.8%, $p < 0.001$, n=17 from 8 mice; The difference between anti-Scramble and anti-Cck after HFS is 30.2 ± 4.0%, $p < 0.001$). In the subsequent experiment, we administered L-365,260 (L365, 250 nM, 0.5 μL), a CCKBR antagonist, into the ACx of mice before HFS in the MGB. As a control, we injected artificial cerebral-spinal fluid (ACSF) instead of CCKBR antagonist. HFS-induced thalamocortical LTP was completely blocked in the L365 application group, whereas no such effect was observed in the ACSF application group (Figure S1D, two-way RM ANOVA, $F[1,32] = 29.3$, $p < 0.001$, pairwise comparison: L365 group, before vs. after HFS, 99.5 ± 0.6% vs. 100.4 ± 3.2%, $p = 0.779$, n=22 from 5 mice; ACSF group, before vs. after HFS, 100.3 ± 0.8% vs. 128.9 ± 4.3%, $p < 0.001$, n=12 from 5 mice; The difference between ACSF group and L365 group after HFS is 28.5 ± 5.4%, $p < 0.001$). Taken together, these findings provide robust evidence supporting that HFS-induced thalamocortical LTP is CCK dependent.

Previous studies have demonstrated that high-frequency activation of entorhinal neurons or entorhino-neocortical CCK projections can elicit CCK release from their terminals [25,26]. Therefore, we investigated whether HFS of MGB or thalamocortical projections could also induce CCK release in the ACx. To directly monitor CCK dynamics, we utilized the G protein-coupled receptor (GPCR) activation-based CCK sensor in ACx [34]. The released CCK binds to the GPCR CCKBR, resulting in increased fluorescence intensity, which can be measured using fiber photometry. In our experimental approach, we injected the AAV9-syn-CCK sensor virus into ACx, and AAV9-Syn-FLEX-ChrimsonR-tdTomato/AAV9-Syn-ChrimsonR-tdTomato into

the MGB of CCK-Cre/CCK-KO mice (Figure 2E upper panel). Effective gene expression was achieved six weeks after the injection (Figure 2E lower panel). We applied a high-frequency laser stimulation (HFLS, 620 nm) to the ACx to activate the thalamocortical terminals. Following HFLS, fluorescence intensity significantly increased in CCK-Cre mice but not in CCK-KO mice (Figures 2F, green and orange traces, Averaged ΔF/F0%: two-way ANOVA followed by Bonferroni multiple comparisons adjustment, significant interaction, $F[1, 28] = 13.25$, $p = 0.001$; before vs. after HFLS in CCK-Cre: -0.002 ± 0.018 vs. 0.163 ± 0.037, $p < 0.001$, n = 16 from 8 mice; before vs. after HFLS in CCK-KO: 0.015 ± 0.019 vs. -0.004 ± 0.039, ns, $p = 0.616$, n = 14 from 7 mice; After HFLS in CCK-Cre vs. CCK-KO: 0.163 ± 0.037 vs. -0.004 ± 0.039, $p = 0.004$). These findings suggest that CCK was released from thalamocortical terminals in response to high-frequency activation. Additionally, we directly applied HFLS to the MGB. The fluorescence intensity exhibited a substantial increase in CCK-Cre mice, whereas no significant change was observed in CCK-KO mice (Figures 2F, red and blue traces, averaged ΔF/F0%: two-way ANOVA followed by Bonferroni multiple comparisons adjustment, significant interaction, $F[1, 39] = 12.70$, $p = 0.001$; before vs. after HFLS in CCK-Cre: -0.003 ± 0.017 vs. 0.396 ± 0.095, $p < 0.001$, n = 21, N = 11; before vs. after HFLS in CCK-KO: 0.000 ± 0.018 vs. -0.031 ± 0.098, ns, $p = 0.723$, n = 20, N = 10; After HFLS in CCK-Cre vs. CCK-KO: 0.396 ± 0.095 vs. -0.031 ± 0.098, $p = 0.003$).

In the previous experiment, the use of two different viruses in the CCK-Cre and CCK-KO mice compromises the suitability of this control. Additionally, CCK is widely distributed in the brain, raising the possibility of CCK being released from other projections via indirect mechanisms, considering the polysynaptic responses that can be elicited in ACx by MGB

stimulation. Furthermore, laser stimulation of the thalamocortical projection may induce antidromic activation in MGB. To address these concerns, we specifically down-regulated Cck expression in MGB neurons and subsequently assessed CCK release after HFS of MGB. We injected the CCK sensor virus and anti-Cck/anti-Scramble shRNAs virus separately into ACx and MGB of C57 mice (Figure 2H upper). After viral expression was achieved (Figure 2H lower panel), we monitored the fluorescence intensity in the ACx before and after HFS at the MGB (Figure 2I upper panel). The fluorescence intensity significantly increased in anti-Scramble group, while no significant change was observed in anti-Cck group (Figures 2I lower, Averaged $\Delta F/F0\%$: two-way ANOVA followed by Bonferroni multiple comparisons adjustment, significant interaction $F[1,41] = 19.70$, $p < 0.001$; before vs. after HFS in anti-Scramble: -0.005 ± 0. 013 vs 0.387 ± 0.064, $p < 0.001$, n=21 from 11 mice; before vs. after HFS in anti-Cck: -0.007 ± 0. 013 vs -0.007 ± 0.063, $p = 0.999$, n=22 from 11 mice; After HFS in anti-Scramble vs. anti-Cck: 0.387 ±0.064 vs -0.007 ± 0.063, $p < 0.001$). These results indicate that HFS of MGB triggers CCK release from direct thalamocortical terminals at the ACx. Thus, HFS of MGB facilitates thalamocortical synaptic plasticity through homosynaptic CCK release.

Cholecystokinin correlates with developmental thalamocortical LTP

The mechanism of LTP underlying thalamocortical plasticity in adult mice is dependent on CCK, which differs from that observed in neonatal brains [1,35]. To investigate the emergence of HFS-induced CCK-dependent plasticity during thalamocortical development, we employed RNAscope in situ hybridization to assess CCK expression levels in MGB neurons in mice across different stages of postnatal life (P14, P20, 8W, 18M, Figure 3A). At P14, we found only a few

population of MGB neurons expressing CCK mRNA, whereas at P20, a significant increase in the number of CCK mRNA-expressing neurons was evident. Subsequently, the number of neurons expressing CCK mRNA showed a slight decline at 8W and a severe decrease at 18M (Figure 3B upper panel, One-way ANVOA, Bonferroni multiple comparisons adjustment: P14 vs. P20, $p < 0.001$; P20 vs. 8W, $p = 1.0$; 8W vs. 18M, $p = 0.018$; 18M vs. CCK-KO, $p = 0.05$; 8W vs. CCK-KO, $p < 0.001$. P14, 57.0 ± 41.5, n = 4 from 2 mice; P20, 276.0 ± 34.2, n = 4 from 2 mice; 8W, 232.3 ± 33.4, n = 4 from 2 mice; 18M, 100 ± 26.9, n = 4 from 2 mice; CCK-KO, 0.0 ± 0.0, n = 8 from 4 mice. The definition of "CCK mRNA-expressing neurons" can be found in the Methods section.). In the CCK-KO young adult control group (8W), no neurons in the MGB exhibited CCK mRNA expression. On the other hand, the normalized CCK mRNA expression level per single neuron declined with age (Figure 3B lower panel, One-way ANVOA, Bonferroni multiple comparisons: P14 vs. 8W, $P < 0.001$; P20 vs. 8W, $P < 0.001$; 18M vs. 8W, $P < 0.001$; P14, 1.048 ± 0.004, n = 228 neurons; P20, 1.042 ± 0.002, n = 1104 neurons; 8W, 1.000 ± 0.002, n = 929 neurons; 18M, 0.949 ± 0.003, n = 400 neurons). Overall, MGB CCK mRNA expression was weak at P14 and reached high levels at P20, decreased slightly at 8W, and markedly dropped at 18M (Figure 3B).

To investigate the correlation between thalamocortical LTP induction and CCK expression, we conducted in-vivo electrophysiology experiments. We selected the P20, 8W, and 18M age groups for our study, excluding P14 mice due to their small body size. As expected, we observed a significant potentiation following HFS of MGB in the 8th week group (same as Figure 1D, Figure 3C middle panel, an increase of 30.0 ± 4.8%, $p<0.001$). Similarly, HFS failed to induce LTP in the aged mice at 18M (Figure 3C lower panel, an increase of 2.9 ± 3.2%, P =

0.380). However, contrary to the RNAscope results, we found that thalamocortical LTP was absent in neonatal mice at P20 (Figure 3C upper panel, increased by 2.2 ± 3.5%, P = 0.542; Figure 3C, two-way RM ANOVA, $F[2,42] = 18.7$, $p < 0.001$, pairwise comparison: before vs. after HFS in P20 mice, 100.0 ± 0.5% vs. 102.2 ± 3.6%, p = 0.542, n = 15 from 10 mice; before vs. after HFS in 8W mice, 100.7 ± 0.4% vs. 130.7 ± 4.8%, $p < 0.001$, n = 13 from 10 mice; before vs. after HFS in 18M mice, 100.5 ± 0.4% vs. 103.3 ± 3.3%, p = 0.380, n=18 from 8 mice). Although the induction level of LTP decreased with CCK mRNA expression in mature mice (8W and 18M; The difference between 8W group and 18M group after HFS is 27.4 ± 5.1%, $p < 0.001$), P20 mice, which exhibited the highest CCK mRNA expression, showed no LTP (difference between 8W group and P20 group after HFS is 28.5 ± 5.3%, $p < 0.001$). This observation led us to speculate that the differential thalamocortical plasticity mechanism between neonatal and adult mice may be attributed to the expression of CCKBR. Therefore, we proceeded to examine the expression level of CCKBR in the ACx during development. As predicted, immunochemistry staining revealed minimal CCKBR signals in P20 mice, while extensive signals were detected in the 8W and 18M groups (Figure 3D). These results indicate the maturation process of the thalamocortical projection during development. The level of HFS-induced thalamocortical LTP correlated with CCK expression in adult mice but not in the neonatal brain, likely due to the limited expression of CCKBR during the critical period.

However, a concern arises in our theory. Despite the low expression of CCK mRNA in aged mice, it is still present. (Figure 3B right panel). In contrast, thalamocortical LTP was barely inducible in aged mice (Figure 3C lower panel), suggesting a lack of CCK release. It is widely recognized that mRNA level does not directly correlate with peptide level. Multiple steps, such

as translation, post-translational modifications, packaging, transportation, and proteolytic processing, involving various enzymes, exist between mRNA expression and neuropeptide release. Apart from the low expression of CCK mRNA, any missing link in this chain could lead to a deficit in CCK release. To investigate whether CCK can be released from aged mice, we employed the CCK sensor to directly detect changes in CCK levels during HFS of the MGB in 18M mice. After the expression of the CCK sensor in aged mice, we monitored fluorescence intensity in the ACx. The signal did not increase following HFS of MGB (Figure 3F, blue). For comparison, we also attached the fluorescence intensity trace of the anti-Scramble group (from Figure 2I, gray) within this Figure (Figures 3F and 3G, Averaged ΔF/F0%: two-way ANOVA followed by Bonferroni multiple comparisons adjustment, significant interaction $F[1,31] = 8.61$, $p = 0.006$; before vs. after HFS in aged mice: 0.014 ± 0. 022 vs 0.052 ±0.098, $p = 0.699$, n=12 from 6 mice; After HFS in aged mice vs. anti-Scramble control: 0.052 ±0.098 vs 0.387 ± 0.074, $p = 0.010$). This result confirms that HFS of MGB fails to trigger CCK release in the aged brain, despite the existence of CCK mRNA. The shortage of CCK could be a contributing factor to the impairment of thalamocortical plasticity in aged mice.

Exogenous CCK application rescues thalamocortical LTP in aged mice and enhances frequency discrimination

Previous studies have demonstrated that age-related impairment of synaptic plasticity, including LTP, leads to hippocampal dysfunction [36], and synaptic plasticity diminishes with age in the thalamocortical pathway of rats [20]. Our findings revealed that thalamocortical LTP could not be induced in aged mice due to the absence of CCK, while CCKBR expression remained intact.

Considering that the loss of LTP could be attributed to decreased CCK release in the thalamocortical pathway, the exogenous infusion of CCK should rescue this age-related impairment. In the electrophysiology experiment, we infused CCK (CCK-4, 0.5 μL, 10 μM, Sigma) or ACSF into the ACx of aged mice (18M), followed by HFS at the MGB (Figures 4A and 4B). The slopes of evoked fEPSPs significantly potentiated after the HFS in the CCK group, but not in the ACSF group (Figure 4C, two-way RM ANOVA, $F[1,22] = 17.9$, $p < 0.001$, pairwise comparison: CCK group, before vs. after, 100.4 ± 0.6% vs. 148.6 ± 10.4%, $p < 0.001$, n = 13 from 6 mice; ACSF group, before vs. after, 98.8 ± 0.7% vs. 103.3 ± 4.9%, $p = 0.404$, n=12 from 7 mice; The difference between CCK group and ACSF group after the intervention is 45.3 ± 15.1%, $p = 0.006$). Exogenous application of CCK restored the lost thalamocortical LTP in the aged mice. Based on previous studies, CCK has been shown to facilitate synaptic plasticity through presynaptic and postsynaptic coactivation [24,25]. Therefore, we further examined whether CCK alone, without MGB stimulation, could induce thalamocortical LTP. We infused CCK-4 into the ACx of adult mice after baseline fEPSP recording. Stimulation was paused for 15 min to allow for CCK-4 degradation, after which recording was resumed. The thalamocortical LTP was not induced by the CCK injection alone (Figure S2A, one-way RM ANOVA, $F[1,19] = 0.003$; pairwise comparison, before vs. after CCK alone, 99.1 ± 0.4% vs. 99.2 ± 1.4%, $p = 0.956$, n = 20 from 5 mice). Evidently, the activation of the thalamocortical pathway is crucial for inducing thalamocortical LTP, and CCK serves as a key modulator in this process.

CCK administration effectively restored thalamocortical LTP in aged brains, indicating its potential therapeutic application in developmental impairments or age-related diseases. Considering that direct stimulation of the MGB is not suitable for clinical treatment, we explored

whether the combination of CCK administration with a natural auditory stimulus could induce thalamocortical plasticity. Initially, we injected the AAV9-Syn-ChrimsonR-tdT virus into the MGB of C57 mice, which labeled the projection from MGB in the ACx (Figure 4D). In the electrophysiology experiment, we infused CCK-4 or ACSF into the ACx and delivered auditory stimulation for 200 trials (0.5 Hz) to the animals (Figure 4E). The fEPSPs in response to laser stimulation in the ACx were recorded before and after the intervention. The thalamocortical LTP was induced in the CCK group, while no significant changes were observed in the ACSF group (Figure 4F, two-way RM ANOVA, $F[1,27] = 30.7$, $p < 0.001$, pairwise comparison: CCK group, before vs. after, 99.9 ± 0.9% vs. 146.1 ± 7.0%, $p < 0.001$, n = 10 from 10 mice; ACSF group, before vs. after, 100.7 ± 0.7% vs. 100.0 ± 5.1%, $p = 0.899$, n=19 from 10 mice; The difference between CCK group and ACSF group after the intervention is 46.1 ± 8.6%, $p < 0.001$). Furthermore, we investigated whether auditory stimulation was necessary for the induction of thalamocortical LTP. Figure S2B demonstrated that CCK-4 alone, without acoustic stimulation, failed to potentiate the neural response to laser in the ACx (Figure S2B, one-way RM ANOVA, $F[1,21] = 0.546$; pairwise comparison, before vs. after CCK alone, 100.3 ± 0.4% vs. 99.0 ± 1.9%, $p = 0.468$, n = 22 from 4 mice). Collectively, these findings suggest a promising therapeutic approach for treating diseases associated with impairments in thalamocortical connectivity.

Auditory thalamocortical plasticity plays a decisive role in inducing precise modifications of cortical neurons, which underlie the frequency-specific plasticity in the auditory cortex [37,38]. Chen et al. demonstrated that optogenetic silencing of the auditory thalamocortical projection impaired auditory decision-making in a frequency-discrimination task [39]. In our subsequent experiment, we employed a prepulse inhibition (PPI) acoustic startle test to assess the

mice's ability to discriminate frequencies (Figure 5A). The level of prepulse inhibition reflects the animals' perception of frequency differences between the background tone and the prepulse tone. A higher PPI indicates a better ability to discriminate between the two frequencies, as exemplified in Figure 5B. It is known that sensory experiences, such as sound exposure, can influence thalamocortical plasticity in adulthood[12,16,21]. After habituation, young adult mice were exposed to tone stimulations (9.8 or 16.4 kHz, which would serve as the background tone in PPI) in a soundproof chamber immediately following bilateral injection of either CCK or ACSF into the ACx through implanted cannulas (Figure 5A). The frequency-discrimination ability was evaluated by comparing the PPIs between the two groups after 24 hours of exposure. As expected, in both ACSF control groups (Figure 5C, 9.8 kHz; Figure 5D, 16.4 kHz, gray lines), mice exhibited a gradual increase in PPI as the frequency difference between the background tone and the prepulse tone increased. The differences between the CCK experimental group and the ACSF control group were primarily observed in discriminating frequencies near the exposed frequency, with a > 18.8% difference for both the 9.8 and 16.4 kHz groups when detecting the prepulse tone at -2% from the exposed frequency (Figure 5C, 9.8 kHz, CCK group, n = 7, ACSF group, n = 7, two-way ANOVA, $p < 0.05$, 32.50 ± 3.86% vs 13.67 ± 2.77%, post-hoc, Tukey test, CCK vs. ACSF, **, $p<0.001$; Figure 5D, 16.4kHz, CCK group, n=7, ACSF group, n=7, two-way ANOVA, $p < 0.05$, 39.15 ± 3.01% vs 15.43 ± 4.97%, post-hoc, Tukey test, CCK vs. ACSF, **, $p < 0.001$). The efficacy of the thalamocortical system reaches a plateau in young adult animals, potentially explaining why the behavior improvement in the CCK-treated group, compared to the control group, was only significant in discriminating the -2% difference. This phenomenon underscores the ability of the auditory thalamocortical system to implement frequency-specific

plasticity in cortical function [37,38]. In fact, this result can also be supported by a pilot study we conducted on rats (Figures S2C-E). We infused CCK into the ACx and delivered a tone stimulus for 200 trials to anesthetized rats. We measured the tuning curves of auditory cortical neurons before and after the intervention. The frequency of the selected exposed tone is a non-characteristic frequency (CF) that elicited a moderate response. Although CCK did not induce a shift in the CF of the tuning curve (Figure S2C), the response threshold to exposed tone was significantly lowered. In contrast, the control group with ACSF infusion did not exhibit a lowered response threshold to the exposed tone (Figure S2D for an example; Figure S2E for group data, 8.66 ± 1.91 dB at exposed frequency, $p < 0.001$; 6.66 ± 2.32 dB $P < 0.001$ and 5.33 ± 1.33 dB, $p < 0.05$ at frequencies of 0.4 octave lower and 0.4 octave higher than the exposed frequency respectively; CCK, n = 15; ACSF n = 12, two-way ANOVA, $p < 0.001$, post hoc: Tukey test, CCK-8S vs. ACSF, *, $p < 0.05$; **, $p < 0.001$). The application of CCK and sound exposure led to a lowered response threshold near the exposed tone, explaining why the behavior improvement was only significant in discriminating the -2% difference.

Age-related atrophy in thalamocortical connectivity contributes to cognitive decline [40]. In our study, we demonstrated deficits in CCK-dependent thalamocortical plasticity in aged mice and successfully restored the plasticity of thalamocortical connectivity by administering exogenous CCK into the ACx. Subsequently, we assessed the performance of aged mice in the PPI test. We examined whether intraperitoneal (i.p.) administration of CCK could enhance their frequency discrimination ability, considering that i.p. is a more feasible therapeutic option than intra-cortical administration. After habituation, 15 C57 aged 18M were i.p. injected with CCK-4 solution (1 mg/kg), while 15 littermate controls received saline injections. Fiber photometry on

CCK sensor-expressing mice confirmed that CCK-4 penetrated the blood-brain barrier and reach ACx (Figures S2F-H, Averaged ΔF/F0% of CCK-Cre mice: two-way ANOVA followed by Bonferroni multiple comparisons adjustment, $F[1,14] = 7.465$, $p = 0.016$, before vs. after CCK-4 treatment: 0.003 ± 0.036 vs. 0.523 ± 0.154, $p = 0.002$, $N = 7$; before vs. after Saline treatment: 0.003 ± 0.032 vs. 0.011 ± 0.135, $p = 0.951$, $N = 9$; After CCK-4 vs. after Saline: 0.523 ± 0.154 vs. 0.011 ± 0.135, $p = 0.025$; Averaged ΔF/F0% of CCK-KO mice: two-way ANOVA followed by Bonferroni multiple comparisons adjustment, $F[1,13] = 22.99$, $p < 0.001$; before vs. after CCK-4 treatment: 0.024 ± 0.037 vs. 0.716 ± 0.122, $p < 0.001$, $N = 7$; before vs. after Saline treatment: 0.025 ± 0.035 vs. 0.009 ± 0.115, $p = 0.877$, $N = 8$; After CCK-4 vs. after Saline: 0.716 ± 0.122 vs. 0.009 ± 0.115, $p = 0.001$). Immediately after the injection, the mice were exposed to tone stimulations (9.8 kHz) in a soundproof chamber (Figure 5E). The PPI test conducted 24 hours after exposure revealed significant differences between the CCK group and the saline groups across almost all tested prepulse frequencies (Figure 5F, two-way ANOVA, test of between-drug effects in frequency-discrimination task: $F[1,28] = 9.572$, $p = 0.004$, CCK group $N = 15$, ACSF group $N = 15$. Bonferroni-adjusted pairwise multiple comparisons with CCK vs. Saline in Δf = **-2%**: 21.8 ± 3.3% vs. 8.7 ± 3.3%, $p = 0.010$; Δf = **-4%**: 33.8 ± 3.8% vs. 17.8 ± 3.8%, $p = 0.006$; Δf = **-8%**: 38.9 ± 4.6% vs. 19.5 ± 4.6%, $p = 0.006$; Δf = **-16%**: 42.7 ± 5.1% vs. 25.3 ± 5.1%, $p = 0.022$; Δf = **-32%**: 50.4 ± 5.5% vs. 32.3 ± 5.5%, $p = 0.027$). The difference in efficacy between exogenous CCK application in young adults (Figures 5H and 5I) and aged animals may be attributed to variations in endogenous CCK expression in these age groups. Overall, our findings suggest that the combination of CCK administration and sound stimulation

holds promise as a potential therapeutic approach for addressing cognitive decline associated with alterations in auditory thalamocortical connectivity or deficits in thalamocortical plasticity.

Discussion

In the present study, we aimed to provide a comprehensive understanding of the role of CCK in age-dependent thalamocortical plasticity and explore potential therapeutic interventions for neurodegenerative deficits associated with thalamocortical neuroplasticity. We demonstrated that HFS in the MGB successfully induced thalamocortical LTP in adult mice, and this LTP was shown to be dependent on CCK. The recurrence of thalamocortical LTP after the neonatal thalamocortical plasticity time window was attributed to the increased expression of CCK and its receptor, CCKBR, during development. In aged mice, the loss of thalamocortical LTP was likely due to the down-regulation of CCK expression and impaired CCK release in the thalamocortical pathway. Therefore, administration of CCK into the ACx of aged mice restored thalamocortical LTP. Notably, auditory exposure following CCK application in the ACx potentiated thalamocortical connectivity and enhanced the mice's frequency discrimination in behavioral experiments.

Thalamocortical Long-term Potentiation

Thalamocortical plasticity plays a crucial role in the development of sensory cortices. Based on previous studies on the development of topographical maps in sensory cortices [35], it has been proposed that the refinement of thalamocortical projections occurs through the activity-

dependent thalamic axon competition for cortical neurons [41]. The switching of NMDA receptor subunits (NR2B to NR2A) on thalamocortical synapses during early development indicates a critical period for NMDA-dependent LTP at these synapses [8]. Correlated pre- and postsynaptic activity contributes to the conversion of thalamocortical silent synapses into functional synapses, thereby facilitating neonatal thalamocortical development [42]. Zhang and colleagues observed that exposing neonatal rats to pulsed monotone stimuli from P9 to P28 resulted in an expansion of the cortical area representing the exposed tones in the ACx of rats [43]. Other studies have shown the existence of thalamocortical plasticity in the adult brain, which can be induced by different protocols [17,20,22].

Consistent with the findings of Heynen and Bear (2001) [22], our results demonstrated that thalamocortical LTP could be induced using the standard protocol of HFS, indicating that thalamocortical synapses retain their plasticity beyond the early critical period as defined by Malenka [1]. In this study, we successfully induced thalamocortical LTP in the ACx of young adult mice with *in-vivo* preparation. This induction of LTP was observed to enhance auditory signal propagation, providing evidence of the functional impact of the HFS-induced thalamocortical plasticity. (Figure 1).

CCK Dependence of Thalamocortical Neuroplasticity

Previous studies have demonstrated the crucial role of CCK in facilitating cortical plasticity in adult rats and mice [24-27]. Additionally, Senatorov and colleagues reported the presence of CCK mRNA in the reciprocally connected areas of the MGB and the ACx, with a high density of CCKBR observed in layer IV of the ACx [31,33]. These findings suggest a potential involvement of

CCK in thalamocortical plasticity. In our present study, we further confirmed that high-frequency laser activation of thalamocortical CCK projection triggered the release of CCK, thereby facilitating thalamocortical LTP (Figures 2B and 2F). In contrast, down-regulation of the Cck expression in MGB neurons resulted in the abolishment of HFS-induced CCK release and subsequent LTP (Figures 2D and 2I). Likewise, administration of a CCKB receptor antagonist blocked thalamocortical LTP in the wild-type mice (Figure S1D), providing additional evidence for the indispensability of CCK in enabling thalamocortical neuroplasticity.

Developmental thalamocortical LTP

In the mouse auditory system, MGB projections enter the subplate area and activate subplate neurons as early as P2 [44,45]. These neurons in the ACx guide thalamocortical projections to layer IV during the first two postnatal weeks. As thalamocortical connections mature, the subplate neurons eventually die off around the fourth postnatal week[46]. Our findings indicate that CCK-dependent plasticity in the auditory thalamocortical pathway (Figure 3C) emerges with a delay of weeks after the initiation of CCK expression in the MGB (Figures 3A and 3B). This delay is likely attributed to the developmental timeline of the postsynaptic CCKBR in the ACx, which is also critical for thalamocortical plasticity (Figure 3D). Our results align with previous research by Hogsden and Dringenberg (2009), showing that rats at approximately 6 weeks of age exhibited the highest level of HFS-induced thalamocortical LTP, which declined with age [20]. We also confirmed that HFS failed to induce thalamocortical LTP in mice older than 18 months, whose CCK mRNA expression in the MGB was significantly down-regulated together with a deficit in CCK release.

CCK administration rescued thalamocortical LTP in aged mice and improved frequency discrimination ability.

Given that aged mice exhibited a deficiency in endogenous CCK but possessed intact CCKBR, we successfully restored the impaired thalamocortical LTP by applying exogenous CCK into the ACx of aged mice (Figure 4C). The combined application of CCK and acoustic stimulation enhanced thalamocortical connectivity (Figure 4F), suggesting a potential therapeutic application.

Auditory cortical plasticity is known to correlate with improved perceptual acuity and learning [17,47], while thalamocortical plasticity is a determinant in the refinement of cortical neurons [37,38]. Inhibition of thalamocortical inputs has been shown to impair frequency-discrimination ability in animals [39]. Our behavioral experiments demonstrated that a combination of passive tone stimulation and CCK infusion into the bilateral auditory cortices of young adult mice significantly increased their frequency-discrimination ability towards the exposed frequency (Figures 5C and 5D), providing further evidence for the rewiring and enhancement of adult thalamocortical connectivity through sensory experiences [11,15,19]. In comparison, passive tone stimulation combined with i.p. administration of CCK in aged mice improved their discrimination ability across all frequencies (Figure 5F), possibly by enhancing diminished thalamocortical communication. More probably, endogenous CCK in young adult animals is sufficient to regulate thalamocortical plasticity, enabling them to adapt to environmental changes. In contrast, aged mice, lacking sufficient endogenous CCK, exhibited increased sensitivity to CCK administration, as indicated by a slightly more intense fluorescence signal in CCKKO mice than CCKCre mice after CCK injection (Figure S2G, CCKKO is 19.3 ± 16.4% greater, although

statistically non-significant). Moreover, CCK-induced cortical LTP was more pronounced in CCKKO mice compared to C57 mice[25].

The potential role of CCK from the thalamocortical pathway in modulating corticocortical plasticity

Exogenous administration of CCK along with tone exposure has been shown to enhance thalamocortical connectivity and improve frequency-discrimination ability. However, it is important to note that the changes observed in ACx may not exclusively result from the alterations at thalamocortical synapses. Heterosynaptic release of CCK from entorhino-neocortical projections has been implicated in modulating corticocortical plasticity and associative memory [25,26,28]. Similarly, thalamocortical projection may also influence intracortical plasticity.

The released CCK activates postsynaptic CCKBR, leading to an increase in intracellular calcium concentration through the activation of phospholipase C [48-50]. This rise in calcium levels could subsequently facilitate the recruitment of AMPA receptors in the postsynaptic neuron [51-55]. In the presence of CCK, several instances of pre- and postsynaptic co-activation can readily induce synaptic plasticity [24,25]. The cortical neural response to MGB stimulation or acoustic stimulation is actually a mix of monosynaptic and polysynaptic excitation and inhibition due to the complexity of the cortical network. Hence, in addition to thalamocortical homosynaptic plasticity, the connectivity of specific intracortical microcircuitry may be modulated via CCK released from thalamocortical projection in a heterosynaptic manner during the activation. Considering the indirect activation, we specifically downregulated the expression of Cck to

confirm that the released CCK was from thalamocortical projection. However, in the current study, we only recorded the fEPSPs in layer IV of ACx, and further investigations are needed to explore this heterosynaptic modulation.

Thalamocortical plasticity in the adult brain has been found to be induced by different methods, reversing the critical periods of the sensory cortices [17,18,56]. Zhou and colleagues reported that exposing juvenile or adult rats to a moderate level of noise exposure could reinstate the high susceptibility of the tonotopic map in the ACx [16]. In a recent study, Blundon and colleagues demonstrated that thalamocortical plasticity could be restored by restricting thalamic adenosine signaling [17]. In parallel, our current study proposes another potential approach to trigger thalamocortical plasticity in the adult brain through CCK administration. The induction of CCK-mediated plasticity holds promise as a possible treatment strategy to enhance the function of late cochlear implants in prelingually deaf children[57] and could serve as a foundation for the development of future non-invasive therapies for age-related hearing loss. Thalamocortical plasticity is now known to participate not only in the refinement of the sensory cortices but also in learning processes [10]. Therefore, our findings may have broader implications across different sensory modalities, including but not limited to perception, learning, and memory formation.

Methods

Animals

In the present study, male mice and rats were used to investigate thalamocortical LTP. Experiments were conducted using C57BL/6 wild-type (C57) mice of different ages (neonatal:

P14 and P20; young adult: 8 weeks, P54 ~ P56; adult: 3 ~ 4 months; aged: 17-20 months), CCK-ires-Cre (Jax#019021, CCK-Cre), CCK-CreERT2 (Jax#012710, CCK-KO) and Sprague-Dawley rats. Animals were housed at 20–24C with 40–60% humidity under a 12-hour-light/12-hour-dark cycle (lights off from 8:00 am to 8:00 pm) with free access to food and water. All experimental procedures were approved by the Animal Subjects Ethics Sub-Committees of the City University of Hong Kong.

Chemicals and Antibodies

For in vivo electrophysiological experiments, CCK-4 (Cat. No. T6515) was purchased from Sigma. CCK-8S (Cat.No. 1166), a selective CCKBR antagonist, L-365, 260 (Cat. No. 2767), DMSO (Cat. No. 3176) were purchased from Tocris Bioscience (Hong Kong, SAR). Artificial cerebrospinal fluid (ACSF, item# 59-7316) was purchased from Harvard Apparatus (U.S.) and used as the solvent for the antagonist above. For immunohistochemical experiments, mouse anti-PSD95 (Invitrogen, #MA1-045, 1:500), goat anti-CCKBR (Invitrogen, #PA5-18384, 1:1000). Secondary antibodies included donkey anti-mouse IgG(H+L) Alexa Fluor 594 (Invitrogen, #A-11058, 1:500), donkey anti-goat IgG(H+L) Alexa Fluor 647 (Invitrogen, #A-21447, 1:500).

Surgery for acute electrophysiological experiments

Mice or rats were anesthetized with urethane sodium (1.8g /kg IP; Sigma, U.S.). Anesthesia was maintained throughout surgery. Atropine sulfate (0.05 mg/kg SC; Sigma, U.S.) was administered 15 min before the induction of anesthesia to inhibit tracheal secretion. The animal was mounted in a stereotaxic frame (Narishige, Japan) and a midline incision was made in the scalp after a liberal application of a local anesthetic (Xylocaine, 2%). A craniotomy was performed (−2 mm

to −4 mm posterior and −1.5 mm to −3 mm ventral to sagittal sutur) to access the auditory cortex, and a hole was drilled in the skull according to the coordinates of the ventral division of the MGB (MGv, AP: -3.2 mm, ML: 2.1 mm, DV: 3.0 mm). The dura mater was minimally opened followed by the silicon oil application to the surface of the brain to prevent drying. The animal's body temperature was maintained at 37-38°C with a feedback-controlled heating pad (RWD, China). After the recording, animals were sacrificed, and the brains were harvested for histological confirmation or further processing.

Virus and retrograde tracer injection

Mice were anesthetized with pentobarbital (50 mg/kg i.p., France) and kept under anesthetic status by supplying one-third of the initial dosage once per hour. For the virus injection into MGB, two small holes were drilled bilaterally in the skull of according to the coordinates of the ventral division of the MGB (MGv, AP: -3.2 mm, ML: 2.1 mm, DV: 3.0 mm). In the optogenetic electrophysiological experiment shown in Figure 2A, AAV9-EFIa-DIO-ChETA-EYFP (300 nL, 6.00E12 gc/mL, Molecular Tools Platform, Canada) was injected into the MGB of CCK-Cre mice at a rate of 30 nL/min (Nanoliter Injector, World Precision Instruments). In the shRNA electrophysiological experiment shown in Figure 2C, rAAV-hSyn-EGFP-5'miR-30a-shRNA(Cck)-3'-miR30a-WPREs (400 nL, 5.63E12 gc/mL, BrainVT, China) or rAAV-hSyn-EGFP-5'miR-30a-shRNA(Scramble)-3'-miR30a-WPREs (400 nL, 6.08E12 gc/mL, BrainVTA, China) was injected into the MGB of C57 mice. In the fiber photometry experiment shown in Figure 2E, AAV9-Syn-FLEX-ChrimsonR-tdTomato (300 nL, 4.00E12 gc/mL, Addgene, U.S.) /AAV9-Syn-ChrimsonR-tdTomato (300 nL, 4.15E12 gc/mL, Addgene, U.S.) was injected into

the MGB of CCK-Cre/CCK-KO mice. In the shRNA fiber photometry experiment shown in Figure 2H, rAAV-hSyn-mCherry-5'miR-30a-shRNA(Cck)-3'-miR30a-WPREs (400 nL, 5.64E12 gc/mL, BrainVTA, China) or rAAV-hSyn-mCherry-5'miR-30a-shRNA(Scarmble)-3'-miR30a-WPREs (400 nL, 5.55E12 gc/mL, BrainVTA, China) was injected into the MGB of C57 mice. In the optogenetic electrophysiological experiment shown in Figures 4D and S2B, AAV9-Syn-ChrimsonR-tdTomato (300 nL, 6.50E12 gc/mL, Addgene, U.S.) was injected into the MGB of C57 mice.

For the ACx injection, two small holes were drilled bilaterally in the skull (AP: −2.8 mm posterior to bregma, ML: −4.2 mm lateral to the midline, DV: 0.9 mm below the pia) to approach ACx to inject AAV9-hSyn-CCK sensor (500 nL, 4.81E12 gc/mL, BrainVTA, China) (Figures 2E, 2H, 3E, and S2F). After injection, animals were sutured and sent back to the home cage for recovery. Antiseptic and analgesic balm was applied on the surface of the wound during the first three days after the surgery.

Auditory, electrical and laser stimuli

Auditory stimuli, including pure tones and noise bursts, were generated by Tucker-Davis Technologies (TDT, U.S.) workstation and delivered through an electrostatic speaker (ED1, TDT). The speaker was placed at 20 cm away from the awake animals or directly to the ear contralateral to the implanted electrodes via a hollow ear bar for the anesthetized animals. The sound pressure level of the speaker was calibrated with a condenser microphone (B&K, Denmark).

The electrical stimulation was generated by an ISO-Flex isolator (A.M.P.I., Israel), which was controlled by a multifunction processor (RX6, TDT). The electrical current pulses for the baseline test were 0.5 ms, 10-100 μA, and presented every 10 s. The high-frequency stimulation (HFS) contained four trains of 10 bursts at 5 Hz with an interval of 10 s between two trains, and each burst consisted of 5 pulses at 100 Hz.

The laser stimulation was produced by a laser generator (Wavelength, 473 nm, 620 nm, CNI laser, China) controlled by RX6 and delivered to the brain by an optic fiber (Thorlabs, U.S.) which was connected to the generator. The output power of the fiber was measured and calibrated by an optical power meter (Item# PM120A, Thorlabs, U.S.) before the insertion into the brain. The laser pulse width was 3 ms, and the interval for baseline testing was 10 s. For the high-frequency laser stimulation (HFLS), the laser stimulation was comprised of four trains of 10 bursts at 5 Hz with an interval of 10 s between the trains, and each burst consisted of five pulses at 80 Hz.

In vivo acute electrophysiological recording

In HFS-induced thalamocortical LTP experiments, two customized microelectrode arrays with four tungsten electrodes each, impedance: 0.5-1.0 MΩ (recording), and 200-500 kΩ (stimulating) (FHC, U.S.), were used for the auditory cortical neuronal activity recording and MGB electrical stimulation, respectively. The electrode arrays were advanced to the brain by two micro-manipulators separately. The recording electrodes were lowered into layer IV of ACx, while the stimulation electrodes were lowered into MGB. The final stimulating and recording positions

were determined by maximizing the cortical field excitatory postsynaptic potential (fEPSP) amplitude triggered by the electrical stimulation in the MGB.

The fEPSPs, which were elicited by 0.5 ms electrical current pulses, were amplified (× 1000) and filtered (1 Hz -5 kHz), recorded at a 25 kHz sampling rate, and stored in a PC by OpenEx software (TDT). Before the recording, an input-output function was measured. A stimulation current, which elicited a fEPSP amplitude 40% of maximum, was chosen for the baseline and after HFS recording. The fEPSPs were collected for 16 min before and 1 h after HFS, respectively. For HFS, each burst includes five 0.5-ms pulses at 100 Hz, and each block consists of 10 bursts at 5 Hz, for a total of 4 blocks with an inter-block interval of 10 s. The current of the pulses that induced 75% of the maximal response was selected from the input-output relationship. The slopes (or amplitude) of the evoked fEPSPs were calculated and normalized by customized MATLAB script, and the group data was plotted as mean ± SEM. In the experiment shown in Figure 1F, 50 noise bursts (Intensity, 70 dB; Duration, 100 ms; Inter-stimulus-interval,10 s) were presented before and after LTP induction session, and multiunit responses to noise bursts of the ACx were recorded. A threshold of 3 standard deviations (SDs) above baseline was set to identify spikes online.

Optogenetic experiments

In the optogenetic experiments, glass pipette electrodes were placed targeting layer IV (350-500μm) of the ACx of mice 4-6 weeks after virus injection. The optic fiber was then inserted into either the ACx next to the electrodes, or MGB. The fEPSPs evoked by laser stimulation were recorded and analyzed in this experiment. The procedure for the HF laser-induced LTP was

similar as previously described in the HFS-induced LTP experiment, except the HF burst containing laser pulses in 80 Hz rather than 100 Hz.

Drug infusion experiments

A glass pipette was placed to ACx adjacent to the recording site for drug application. The tips of glass pipettes were covered by 0.1 μL silicone oil to avoid leaking.

In the antagonist infusion experiments, L-365,260 (250 nM in 5% DMSO, 0.5 μL, tocris) was injected by micro-injector, before the HFS, within 5 min. ACSF (5% DMSO) was injected as a control. In the CCK infusion experiments, CCK-4 (10 μM, 0.5 μL , Sigma) was injected by micro-injector within 5 min. ACSF was injected as a control. In the rat experiments, CCK-8S (1 μM, 1 μL, tocris) or ACSF was infused into the ACx.

Auditory tuning curve test on rats

In the tuning curve test, tones spanning 6 octaves (0.75-48 kHz, 0.2-0.3 octave spacing) and 60 dB (10-70 dB, 5-10 dB spacing) of 100 ms duration were presented every 500 ms in a pseudo-random sequence before and after the infusion and LFS to measure the receptive field of cortical neurons. For the infusion and LFS protocol, CCK-8S (1 μM, 1 μL) or ACSF was infused locally near the recording site, and non-characteristic frequency (non-CF) pure tone stimuli, one octave within the CF, were presented once per 2 s for 200 trails, 5 mins after the infusion. The 30 ms before the onset was considered as the baseline and the 30 ms after the onset of each tone was considered as onset response. The potential tone response bins, of which the firing rates were larger than the averaged firing rate of all the baseline bins plus 3 standard deviations of the firing

rates of these baseline bins (mean+3SD), were considered to have tone response. The tuning curve was determined as the lowest intensity, which had responses to the tone, and characteristic frequency (CF) was the middle frequency at that intensity. To quantify the changes in the tuning curve, we used the frequency responding threshold as the indicator of the change. The data were plotted as mean ± SEM. After the recording, animals were sacrificed, and the brains were harvested for histological confirmation or immunostaining.

Fiberphotometry

This GPCR activation-based CCK sensor, GRABCCK, was developed by inserting a circular-permutated green fluorescent protein (cpEGFP) into the intracellular domain of CCKBR[34]. When the endogenous or exogenous ligand (CCK) binds to the CCKBR, a conformational change in cpEGFP will happen as well as an increase in fluorescence intensity, and the CCK activity could be visualized in vivo. Six-week after CCK-sensor virus injection, a craniotomy was performed to access the auditory cortex (-2 mm to -4 mm posterior and -1.5 mm to -3 mm ventral to sagittal suture), and the dura mater was opened. An optic fiber (400 µm diameter, 0.22 NA, Thorlabs, Newton, NJ) was lowered into the auditory cortex (200-300 µm from the brain surface) to record the signal of the CCK sensor. Before signal recording, the optic fiber was lowered to the brain surface at different sites to confirm the best site for the recording, where we could capture the strongest fluorescence signal of CCK sensor. This optic fiber cannula was attached to a single fluorescent MiniCube (Doric Lenses, Quebec, QC, Canada) with built-in dichroic mirrors and LED light sources through a fiber patch cord. The excitation light at 470 and 405 nm were released by two fiber-coupled LEDs (M470F3 and M405FP1, Thorlabs) and were sinusoidally

modulated at 210 and 330 Hz, respectively. The 473 nm channel is the $GRAB_{CCK}$ channel and the 405nm channel is employed as the isosbestic control channel. An LED driver (LEDD1B, Thorlabs) coupled to the RZ5D processor (TDT, Alachua, FL) managed the excitation light's intensity through the software Synapse. The emission fluorescence was captured and transmitted by a bandpass filter in the MiniCube. To avoid photobleaching, the excitation light intensity at the tip of the patch cord's tip was adjusted to less than 30 μW. The fluorescent signal was then detected, amplified, and transformed into an analog signal by the photoreceiver (Doric Lenses). The analog signal was then digitalized by the RZ5D processor and subjected to a 1 kHz low-pass analysis using Synapse software.

The fluorescent signal was recorded 25s before and 60s after the HFLS (5~10 mW, 635 nm) or HFS application.

For the experiments in Figure S2G, we measured the CCK sensor activities before and after the CCK-4 i.p. application in different type of mice. CCK-4 (1 mg/kg, in 2% DMSO, 8% ethylene glycol, 1% Tween-80, 89% saline) or Saline (0.15 ~ 0.20 mL, in 2% DMSO, 8% ethylene glycol, 1% Tween-80) was i.p. injected. The fluorescent signal was recorded 120s before and 200s after the drug administration.

Fiber Photometry Analysis.

Analysis of the signal was done by the custom-written MATLAB (Mathworks) codes. We first extracted the signal of the 473nm and 405nm channels corresponding to the defined periods before and after each stimulus or drug injection. A fitted 405 nm signal was created by regressing the 405nm channel onto a linear fit of its respective 473 channel (MATLAB *polyfit*

function). The fluorescence change (ΔF/F) was then calculated with the formula (473 nm signal − fitted 405 nm signal)/ fitted 405 nm signal.

Immunohistochemistry

Mice were anesthetized by an overdose of pentobarbital sodium and transcardially perfused with 30 mL cold phosphate-buffered saline (PBS) and 30 mL 4% (w/v) paraformaldehyde (PFA) in PBS. Brain tissue was removed and post-fixed overnight in 4% PFA in PBS at 4°C, and treated with 30% (w/v) sucrose in PBS at 4°C for 2 days. Coronal sections of 50 μm thickness were cut on a cryostat (Epredia CryoStar HM525 NX Cryostat) using OCT and preserved with antifreeze buffer (20% (v/v) glycerol and 30% (v/v) ethylene glycol diluted in PBS) at −20°C.

Brain sections were washed 3 times with PBS before incubated in blocking buffer containing 5% (v/v) normal goat serum (or 5% (w/v) bovine serum albumin if the host of primary antibody is goat) with 0.3% (v/v) Triton X-100 in PBS (PBST) for 2h at room temperature and then incubated with primary antibodies in blocking buffer for 36h at 4°C. The primary antibodies used were: mouse anti-PSD95 (Invitrogen, #MA1-045, 1:500), goat anti-CCKBR (Invitrogen, #PA5-18384, 1:1000). After 3 washes in PBS, sections were incubated with fluorescently-conjugated secondary antibodies: donkey anti-mouse IgG(H+L) Alexa Fluor 594 (Invitrogen, #A-11058, 1:500), donkey anti-goat IgG(H+L) Alexa Fluor 647 (Invitrogen, #A-21447, 1:500) in PBST at room temperature for 2.5h. Next, sections were incubated in DAPI (Chem Cruz, #SC3598) for 5 min, washed several times and mounted with 70% (v/v) glycerol in PBS on slides. Images of immunostained sections were acquired on Nicon confocal microscope and processed with NIS element (Nicon) and ImageJ (NIH). For the colocalization analysis in Figure

2A, we firstly merged channels of virus AAV9-EFIa-DIO-ChETA-EYFP (green) and PSD95 (red) and the co-labeled yellow areas are considered as CCK-positive terminals. The areas were filtered by Color Threshold and then merged with CCKBR channel (magenta).

RNAscope in situ hybridization

Coronal brain sections (20 μm) were prepared with the same methods as tissue used for immunohistochemistry (see above). Using mouse specific CCK probe (ACDbio, #402271) and RNAscope reagent kit-RED (ACDbio, #322350), we performed chromogenic in situ hybridization according to the manufacturer's instructions for fixed frozen sections. Briefly, washed sections were baked for 30min at 60°C, then fixed in 4% PFA in PBS for 15min at 4°C and dehydrated in successive 5-min baths of ethanol (50, 75, 100%). After drying, three steps of pretreatment were performed, including a 10-min hydrogen peroxide treatment, a 15-min target retrieval step in boiling solution, and a 16-min protease digestion step at 40°C. After creating hydrophobic barrier around the perimeter of each section, hybridization with CCK probe was performed for 2h at 40°C, followed by six steps of amplification. Two washes of 2 min were applied after hybridization step and each amplification step. Fast Red was then used as a chromogen for the exposure step for 10 min at room temperature. After washing in water, slides were counterstained with freshly diluted hematoxylin, washed again and dried, then mounted with Vectamount (ACObio, #321584) on SuperFrost Plus slides (Fisher Scientific, #12-550-15).

We understand that the in situ hybridization using fluorescent assays can achieve higher sensitivity, however, our objective in assessing CCK mRNA expression level was to compare the differences across several developmental stages. Therefore, we applied the identical parameters

for imaging and image analysis to ensure accurate comparisons. Brightfield images were acquired using a Nikon Eclipse Ni-E upright microscope. Semi-quantitative analysis of the images was performed employing Fiji ImageJ. ROI was delineated separately for each slice, focusing on the MGv region. The background was subtracted using the Color Deconvolution with the same user-defined values for all the calculated images. Images from the signal channel were first converted to the 8-bit grayscale before applying a threshold as a criterion for binarization, where signals equal to or above the threshold were considered positive. It should be noted that the positive cells we defined here are based on this criterion rather than an absolute definition, and the specific threshold value was appropriately chosen to identify the most of CCK positive neurons in the adult group. Overlapping cells were then separated using the Watershed segmentation function prior to running the Analyze Particles tool for cell counting. The signal intensity of each single cell was then measured on the 8-bit grayscale images, according to the location and area of the positive cells confirmed in the binary images. The CCK mRNA intensity of single cell was normalized to the average CCK expression of all the MGv neurons from 8-week mice.

Cannula implantation

C57 mice were anesthetized, and the scalp was opened, as mentioned above. Two small holes were prepared bilaterally based on the location of the primary ACx (AP: -3.0 mm, ML: 4 mm, DV: 1.2 mm). Drug injection cannulas with metallic caps and dummies (Length: 6 mm, Diameter: 0.6 mm., RWD, China) were inserted into the primary ACx bilaterally and then fixed with C&B-MetaBond adhesive luting cement (Parkell, U.S.) and dental cement (Mega Press,

German). After the implantation, the animals were sent back to their home cages for recovery. Antiseptic and analgesic balm was applied on the surface of the wound on the first three days after the surgery.

Frequency discrimination test

For young adult mice group shown in Figures 5A-D:

Prepulse inhibition of the acoustic startle response test was adopted to examine the frequency discrimination ability of mice in CCK-8S injection group and ACSF control group. In the test, three customized soundproof chambers equipped with vibration sensors on the bottoms for the startle reflex detection, MF-1 multi-field magnetic speakers for tone presentation and high-power tweeter speakers for startle white noise presentation. Three days after the cannula implantation surgery, mice were placed into the self-designed plastic tubes individually with open slots on both sides and front for habituation for 5-10 min every day for 3 days. The mice were then randomly separated into two groups, one CCK-8S infusion group, and one ACSF infusion control group. CCK-8S (10 nM, 1 μL) or ACSF (1 μL) was infused by microinjector at the speed of 0.2 μL/min bilaterally into the auditory cortices. Five minutes after the injection, mice were placed in the tubes and exposed to pure-tone stimulation for 0.5 h in the sound-proof chamber. For the tone exposure protocol, a pure tone of 9.8 kHz or 16.4 kHz (Intensity, 70 dB; duration, 100 ms) was used. The tone exposure consisted of 900 trains with an inter-tone interval of 2s. Each train contained 5 tones presented at 5 Hz. Mice were restrained into the tubes again for the startle test at 24 h after the exposure. The tubes were stabilized on the vibration sensors in the sound-proof chamber during the experiment. The startle reflexes were detected by the sensors

and then amplified and recorded by TDT. The whole experiment was divided into 4 blocks; a background tone (9.8 kHz or 16.4 kHz) was continuously presented at 70 dB throughout the experiment. Block 1 was a 5 min acclimation period in which only the background tone was presented. Block 2 contained 9 startle-only trials in which a white noise burst of 120 dB intensity and 20 ms duration was presented. Block 3 consisted of prepulse inhibition trials in a pseudorandom order. Each prepulse trial consisted of a 80 ms prepulse at 70 dB (pure-tone frequency was 0%, 2%, 4%, 8%, 16%, or 32% lower than the background tone, Δf), followed by a 20 ms white-noise startle pulse at 120 dB, and then return to the background tone after the startle. Every trial in block 3 was presented 15 times. Block 4 was identical with Block 2, and it was used to detect any habituation within the experiment. The inter-trial interval was 10-20 s. The startle reflex was measured as the peak-to-peak amplitude of the raw waveform detected by the sensor. Prepulse inhibition percentage was calculated from block 3 data as follows: [1 – (prepulse trial/Δf=0% prepulse trial)] × 100, and the data was plotted as mean ± SEM. Startle reflex amplitude in Block 2 and Block 4 were compared with each other as an internal control for startle attenuation over the whole experiment. Mice with statistically different performance in Block 2 and Block 4 were removed from the analysis.

For aged mice group shown in Figures 5E and F:

Thirty aged C57 mice of 17-19 months were divided into two groups: Experiment group (CCK-4) and their littermate control group (saline).

The PPI protocol was the same except i.p. CCK-4 (1 mg/kg, in 2% DMSO, 8% ethylene glycol, 1% Tween-80) or Saline (2% DMSO, 8% ethylene glycol, 1% Tween-80) injection instead of

directly delivering the drug into ACx by implanted cannula. 9.8 kHz was used as the background tone and the exposed tone. Tone exposure session consisted of 300 trains with an inter-tone interval of 2 s. Each train included 5 tones (9.8k Hz, 100 ms) presented at 5 Hz. Since the half-life of CCK-4 is short, CCK-4 injection accompanied by pure tone exposure was performed 3 times in D3.

Data analysis

All data are presented as mean ± SEM, and n represents the number of stimulation-recording sites or and N represents the number of animals in each experiment. All statistical analyses (one-way ANOVA or two-way RM ANOVA) were done in SPSS (IBM, USA). Pairwise comparisons were adjusted by Bonferroni correction. Tukey test was used in behavioral study for the post-hoc test. P values < 0.05 were considered statistically significant.

Data Availability

Further information and requests for resources and reagents should be directed to and will be fulfilled by the Lead Contact, Jufang He (jufanghe@cityu.edu.hk)

Acknowledgments:

We thank Prof. Tomas Hökfelt (Karolinska Institutet) and Prof. Bin Hu (Calgary) for critical reviews, and Prof. Kuan-Hong Wang (Rochester), Prof. Xiaomin Zhou (East China Normal University), and Prof. Jan Schnupp (CityU) critical comments on Jingu Feng's Ph.D. thesis (City University of Hong Kong, 2018), which forms part of the current manuscript. We thank Prof.

Yulong Li (Peking University) for providing the CCK-sensor virus. This work was supported by Hong Kong Research Grants Council, and Health and Medical Research Fund, Innovation and Technology Fund (C1014-15G, MRP/101/17X, MPF/053/18X, 08194106, 03141196, 01121906, 11101215M, 11166316M, 11102417M, 11101818M). We also thank the following charitable foundations for their generous support: Wong Chun Hong, Charlie Lee Charitable Foundation, Fong Shu Fook Tong Foundation, and Croucher Foundation.

Author Contributions: JYF, XL, XC, JFH designed the experiments; XL, JYF, MFZ, DXZ, XC collected and analyzed the in-vivo physiology data; XL, XHH, MYC, XW, TC collected and analyzed the data of fiber photometry experiments; PPZ, JYF, PJ, ZJX, XL collected and analyzed the behavioral data; TC, XJZ, JYF, LH, XW, XL collected and analyzed the anatomy data; XHH and TC collected and analyzed the RNAscope data; LX, JYF, JFH wrote the manuscript. XL, LH, STB, XW, HXH, XC, TC, PPZ edited the paper.

Declaration of Interests: The authors declare no competing interests.

References:

1. Crair, M.C., and Malenka, R.C. (1995). A critical period for long-term potentiation at thalamocortical synapses. Nature *375*, 325-328. 10.1038/375325a0.
2. Schlaggar, B.L., Fox, K., and O'Leary, D.M. (1993). Postsynaptic control of plasticity in developing somatosensory cortex. Nature *364*, 623-626. 10.1038/364623a0.
3. Datwani, A., Iwasato, T., Itohara, S., and Erzurumlu, R.S. (2002). NMDA Receptor-Dependent Pattern Transfer from Afferents to Postsynaptic Cells and Dendritic Differentiation in the Barrel Cortex. Molecular and Cellular Neuroscience *21*, 477-492. https://doi.org/10.1006/mcne.2002.1195.
4. Iwasato, T., Erzurumlu, R.S., Huerta, P.T., Chen, D.F., Sasaoka, T., Ulupinar, E., and Tonegawa, S. (1997). NMDA Receptor-Dependent Refinement of Somatotopic Maps. Neuron *19*, 1201-1210. https://doi.org/10.1016/S0896-6273(00)80412-2.

5. Zhang, L.I., Bao, S., and Merzenich, M.M. (2002). Disruption of primary auditory cortex by synchronous auditory inputs during a critical period. Proceedings of the National Academy of Sciences *99*, 2309-2314.
6. Barth, A.L., and Malenka, R.C. (2001). NMDAR EPSC kinetics do not regulate the critical period for LTP at thalamocortical synapses. Nature Neuroscience *4*, 235-236. 10.1038/85070.
7. Malenka, R.C., and Bear, M.F. (2004). LTP and LTD: An Embarrassment of Riches. Neuron *44*, 5-21. https://doi.org/10.1016/j.neuron.2004.09.012.
8. Liu, X.B., Murray, K.D., and Jones, E.G. (2004). Switching of NMDA receptor 2A and 2B subunits at thalamic and cortical synapses during early postnatal development. J Neurosci *24*, 8885-8895. 10.1523/jneurosci.2476-04.2004.
9. Yu, X., Chung, S., Chen, D.-Y., Wang, S., Dodd, Stephen J., Walters, Judith R., Isaac, John T.R., and Koretsky, Alan P. (2012). Thalamocortical Inputs Show Post-Critical-Period Plasticity. Neuron *74*, 731-742. https://doi.org/10.1016/j.neuron.2012.04.024.
10. Biane, Jeremy S., Takashima, Y., Scanziani, M., Conner, James M., and Tuszynski, Mark H. (2016). Thalamocortical Projections onto Behaviorally Relevant Neurons Exhibit Plasticity during Adult Motor Learning. Neuron *89*, 1173-1179. https://doi.org/10.1016/j.neuron.2016.02.001.
11. Audette, N.J., Bernhard, S.M., Ray, A., Stewart, L.T., and Barth, A.L. (2019). Rapid Plasticity of Higher-Order Thalamocortical Inputs during Sensory Learning. Neuron *103*, 277-291.e274. https://doi.org/10.1016/j.neuron.2019.04.037.
12. Oberlaender, M., Ramirez, A., and Bruno, R.M. (2012). Sensory experience restructures thalamocortical axons during adulthood. Neuron *74*, 648-655. 10.1016/j.neuron.2012.03.022.
13. Montey, K.L., and Quinlan, E.M. (2011). Recovery from chronic monocular deprivation following reactivation of thalamocortical plasticity by dark exposure. Nature Communications *2*, 317. 10.1038/ncomms1312.
14. Mainardi, M., Landi, S., Gianfranceschi, L., Baldini, S., De Pasquale, R., Berardi, N., Maffei, L., and Caleo, M. (2010). Environmental enrichment potentiates thalamocortical transmission and plasticity in the adult rat visual cortex. Journal of neuroscience research *88*, 3048-3059.
15. Rodríguez, G., Chakraborty, D., Schrode, K.M., Saha, R., Uribe, I., Lauer, A.M., and Lee, H.K. (2018). Cross-Modal Reinstatement of Thalamocortical Plasticity Accelerates Ocular Dominance Plasticity in Adult Mice. Cell Rep *24*, 3433-3440.e3434. 10.1016/j.celrep.2018.08.072.
16. Zhou, X., Panizzutti, R., de Villers-Sidani, E., Madeira, C., and Merzenich, M.M. (2011). Natural restoration of critical period plasticity in the juvenile and adult primary auditory cortex. J Neurosci *31*, 5625-5634. 10.1523/jneurosci.6470-10.2011.
17. Blundon, J.A., Roy, N.C., Teubner, B.J.W., Yu, J., Eom, T.Y., Sample, K.J., Pani, A., Smeyne, R.J., Han, S.B., Kerekes, R.A., et al. (2017). Restoring auditory cortex plasticity in adult mice by restricting thalamic adenosine signaling. Science *356*, 1352-1356. 10.1126/science.aaf4612.
18. Chung, S., Jeong, J.H., Ko, S., Yu, X., Kim, Y.H., Isaac, J.T.R., and Koretsky, A.P. (2017). Peripheral Sensory Deprivation Restores Critical-Period-like Plasticity to Adult Somatosensory Thalamocortical Inputs. Cell Rep *19*, 2707-2717. 10.1016/j.celrep.2017.06.018.
19. Chun, S., Bayazitov, I.T., Blundon, J.A., and Zakharenko, S.S. (2013). Thalamocortical Long-Term Potentiation Becomes Gated after the Early Critical Period in the Auditory Cortex. The Journal of Neuroscience *33*, 7345-7357. 10.1523/jneurosci.4500-12.2013.
20. Hogsden, J.L., and Dringenberg, H.C. (2009). Decline of long-term potentiation (LTP) in the rat auditory cortex in vivo during postnatal life: Involvement of NR2B subunits. Brain Research *1283*, 25-33. https://doi.org/10.1016/j.brainres.2009.06.001.

21. Speechley, W.J., Hogsden, J.L., and Dringenberg, H.C. (2007). Continuous white noise exposure during and after auditory critical period differentially alters bidirectional thalamocortical plasticity in rat auditory cortex in vivo. Eur J Neurosci *26*, 2576-2584. 10.1111/j.1460-9568.2007.05857.x.
22. Heynen, A.J., and Bear, M.F. (2001). Long-term potentiation of thalamocortical transmission in the adult visual cortex in vivo. J Neurosci *21*, 9801-9813. 10.1523/jneurosci.21-24-09801.2001.
23. Cooke, S.F., and Bear, M.F. (2010). Visual experience induces long-term potentiation in the primary visual cortex. J Neurosci *30*, 16304-16313. 10.1523/jneurosci.4333-10.2010.
24. Li, X., Yu, K., Zhang, Z., Sun, W., Yang, Z., Feng, J., Chen, X., Liu, C.-H., Wang, H., Guo, Y.P., and He, J. (2014). Cholecystokinin from the entorhinal cortex enables neural plasticity in the auditory cortex. Cell Research *24*, 307-330. 10.1038/cr.2013.164.
25. Chen, X., Li, X., Wong, Y.T., Zheng, X., Wang, H., Peng, Y., Feng, H., Feng, J., Baibado, J.T., Jesky, R., et al. (2019). Cholecystokinin release triggered by NMDA receptors produces LTP and sound-sound associative memory. Proc Natl Acad Sci U S A *116*, 6397-6406. 10.1073/pnas.1816833116.
26. Li, X., He, L., Hu, X., Huang, F., Wang, X., Chen, M., Yoon, E.G., Bello, S.T., Chen, T., Chen, X., et al. (2023). Interhemispheric cortical long-term potentiation in the auditory cortex requires heterosynaptic activation of entorhinal projection. iScience *26*, 106542. https://doi.org/10.1016/j.isci.2023.106542.
27. Zhang, Z., Zheng, X., Sun, W., Peng, Y., Guo, Y., Lu, D., Zheng, Y., Li, X., Jendrichovsky, P., Tang, P., et al. (2020). Visuoauditory Associative Memory Established with Cholecystokinin Under Anesthesia Is Retrieved in Behavioral Contexts. J Neurosci *40*, 2025-2037. 10.1523/jneurosci.1673-19.2019.
28. Sun, W., Wu, H., Peng, Y., Zheng, X., Li, J., Zeng, D., Tang, P., Zhao, M., Feng, H., Li, H., et al. (2024). Heterosynaptic plasticity of the visuo-auditory projection requires cholecystokinin released from entorhinal cortex afferents. eLife *13*, e83356. 10.7554/eLife.83356.
29. Feng, H., Su, J., Fang, W., Chen, X., and He, J. (2021). The entorhinal cortex modulates trace fear memory formation and neuroplasticity in the mouse lateral amygdala via cholecystokinin. elife *10*, e69333.
30. Burgunder, J.M., and Young, W.S., 3rd (1988). The distribution of thalamic projection neurons containing cholecystokinin messenger RNA, using in situ hybridization histochemistry and retrograde labeling. Brain Res *464*, 179-189. 10.1016/0169-328x(88)90024-1.
31. Senatorov, V.V., Trudeau, V.L., and Hu, B. (1997). Expression of cholecystokinin messenger RNA in reciprocally-connected auditory thalamus and cortex in the rat. Neuroscience *79*, 915-921. 10.1016/s0306-4522(97)00045-6.
32. Fallon, J.H., and Seroogy, K.B. (1984). Visual and auditory pathways contain cholecystokinin: Evidence from immunofluorescence and retrograde tracing. Neuroscience Letters *45*, 81-87. https://doi.org/10.1016/0304-3940(84)90333-1.
33. Zarbin, M.A., Innis, R.B., Wamsley, J.K., Snyder, S.H., and Kuhar, M.J. (1983). Autoradiographic localization of cholecystokinin receptors in rodent brain. J Neurosci *3*, 877-906. 10.1523/jneurosci.03-04-00877.1983.
34. Wang, H., Qian, T., Zhao, Y., Zhuo, Y., Wu, C., Osakada, T., Chen, P., Chen, Z., Ren, H., and Yan, Y. (2023). A tool kit of highly selective and sensitive genetically encoded neuropeptide sensors. Science *382*, eabq8173.
35. Barkat, T.R., Polley, D.B., and Hensch, T.K. (2011). A critical period for auditory thalamocortical connectivity. Nature Neuroscience *14*, 1189-1194. 10.1038/nn.2882.

919 36. Deupree, D.L., Bradley, J., and Turner, D.A. (1993). Age-related alterations in potentiation in the
920 CA1 region in F344 rats. Neurobiology of Aging *14*, 249-258. https://doi.org/10.1016/0197-
921 4580(93)90009-Z.
922 37. Liu, X., Basavaraj, S., Krishnan, R., and Yan, J. (2011). Contributions of the thalamocortical
923 system towards sound-specific auditory plasticity. Neuroscience & Biobehavioral Reviews *35*,
924 2155-2161. https://doi.org/10.1016/j.neubiorev.2011.02.010.
925 38. Jafari, M.R., Zhang, Y., and Yan, J. (2007). Multiparametric changes in the receptive field of
926 cortical auditory neurons induced by thalamic activation in the mouse. Cereb Cortex *17*, 71-80.
927 10.1093/cercor/bhj125.
928 39. Chen, L., Wang, X., Ge, S., and Xiong, Q. (2019). Medial geniculate body and primary auditory
929 cortex differentially contribute to striatal sound representations. Nat Commun *10*, 418.
930 10.1038/s41467-019-08350-7.
931 40. Hughes, E.J., Bond, J., Svrckova, P., Makropoulos, A., Ball, G., Sharp, D.J., Edwards, A.D., Hajnal,
932 J.V., and Counsell, S.J. (2012). Regional changes in thalamic shape and volume with increasing
933 age. Neuroimage *63*, 1134-1142. 10.1016/j.neuroimage.2012.07.043.
934 41. Goodman, C.S., and Shatz, C.J. (1993). Developmental mechanisms that generate precise
935 patterns of neuronal connectivity. Cell *72*, 77-98. https://doi.org/10.1016/S0092-
936 8674(05)80030-3.
937 42. Isaac, J.T.R., Crair, M.C., Nicoll, R.A., and Malenka, R.C. (1997). Silent Synapses during
938 Development of Thalamocortical Inputs. Neuron *18*, 269-280. https://doi.org/10.1016/S0896-
939 6273(00)80267-6.
940 43. Zhang, L.I., Bao, S., and Merzenich, M.M. (2001). Persistent and specific influences of early
941 acoustic environments on primary auditory cortex. Nature Neuroscience *4*, 1123-1130.
942 10.1038/nn745.
943 44. Viswanathan, S., Bandyopadhyay, S., Kao, J.P., and Kanold, P.O. (2012). Changing microcircuits in
944 the subplate of the developing cortex. J Neurosci *32*, 1589-1601. 10.1523/jneurosci.4748-
945 11.2012.
946 45. Zhao, C., Kao, J.P., and Kanold, P.O. (2009). Functional excitatory microcircuits in neonatal cortex
947 connect thalamus and layer 4. J Neurosci *29*, 15479-15488. 10.1523/jneurosci.4471-09.2009.
948 46. Bandiera, S., and Molnár, Z. (2022). Development of the Thalamocortical Systems. In The
949 Thalamus, M.M. Halassa, ed. (Cambridge University Press), pp. 139-162. DOI:
950 10.1017/9781108674287.008.
951 47. Recanzone, G.H., Schreiner, C.E., and Merzenich, M.M. (1993). Plasticity in the frequency
952 representation of primary auditory cortex following discrimination training in adult owl monkeys.
953 J Neurosci *13*, 87-103. 10.1523/jneurosci.13-01-00087.1993.
954 48. Lee, Y.M., Beinborn, M., McBride, E.W., Lu, M., Kolakowski, L.F., Jr., and Kopin, A.S. (1993). The
955 human brain cholecystokinin-B/gastrin receptor. Cloning and characterization. J Biol Chem *268*,
956 8164-8169.
957 49. Detjen, K., Yule, D., Tseng, M.-J., Williams, J.A., and Logsdon, C.D. (1997). CCK-B receptors
958 produce similar signals but have opposite growth effects in CHO and Swiss 3T3 cells. American
959 Journal of Physiology-Cell Physiology *273*, C1449-C1457.
960 50. Yule, D.I., Baker, C.W., and Williams, J.A. (1999). Calcium signaling in rat pancreatic acinar cells: a
961 role for Gαq, Gα11, and Gα14. American Journal of Physiology-Gastrointestinal and Liver
962 Physiology *276*, G271-G279.

963 51. Lynch, G., Larson, J., Kelso, S., Barrionuevo, G., and Schottler, F. (1983). Intracellular injections of
964 EGTA block induction of hippocampal long-term potentiation. Nature *305*, 719-721.
965 52. Malenka, R.C., Kauer, J.A., Zucker, R.S., and Nicoll, R.A. (1988). Postsynaptic calcium is sufficient
966 for potentiation of hippocampal synaptic transmission. Science *242*, 81-84.
967 53. Bredt, D.S., and Nicoll, R.A. (2003). AMPA Receptor Trafficking at Excitatory Synapses. Neuron
968 *40*, 361-379. https://doi.org/10.1016/S0896-6273(03)00640-8.
969 54. Wang, Y., Wu, J., Rowan, M.J., and Anwyl, R. (1996). Ryanodine produces a low frequency
970 stimulation-induced NMDA receptor-independent long-term potentiation in the rat dentate
971 gyrus in vitro. J Physiol *495 (Pt 3)*, 755-767. 10.1113/jphysiol.1996.sp021631.
972 55. Berridge, M.J. (1998). Neuronal calcium signaling. Neuron *21*, 13-26.
973 56. Zhu, X., Wang, F., Hu, H., Sun, X., Kilgard, M.P., Merzenich, M.M., and Zhou, X. (2014).
974 Environmental acoustic enrichment promotes recovery from developmentally degraded
975 auditory cortical processing. J Neurosci *34*, 5406-5415. 10.1523/jneurosci.5310-13.2014.
976 57. Niparko, J.K., Tobey, E.A., Thal, D.J., Eisenberg, L.S., Wang, N.Y., Quittner, A.L., and Fink, N.E.
977 (2010). Spoken language development in children following cochlear implantation. Jama *303*,
978 1498-1506. 10.1001/jama.2010.451.

979

980

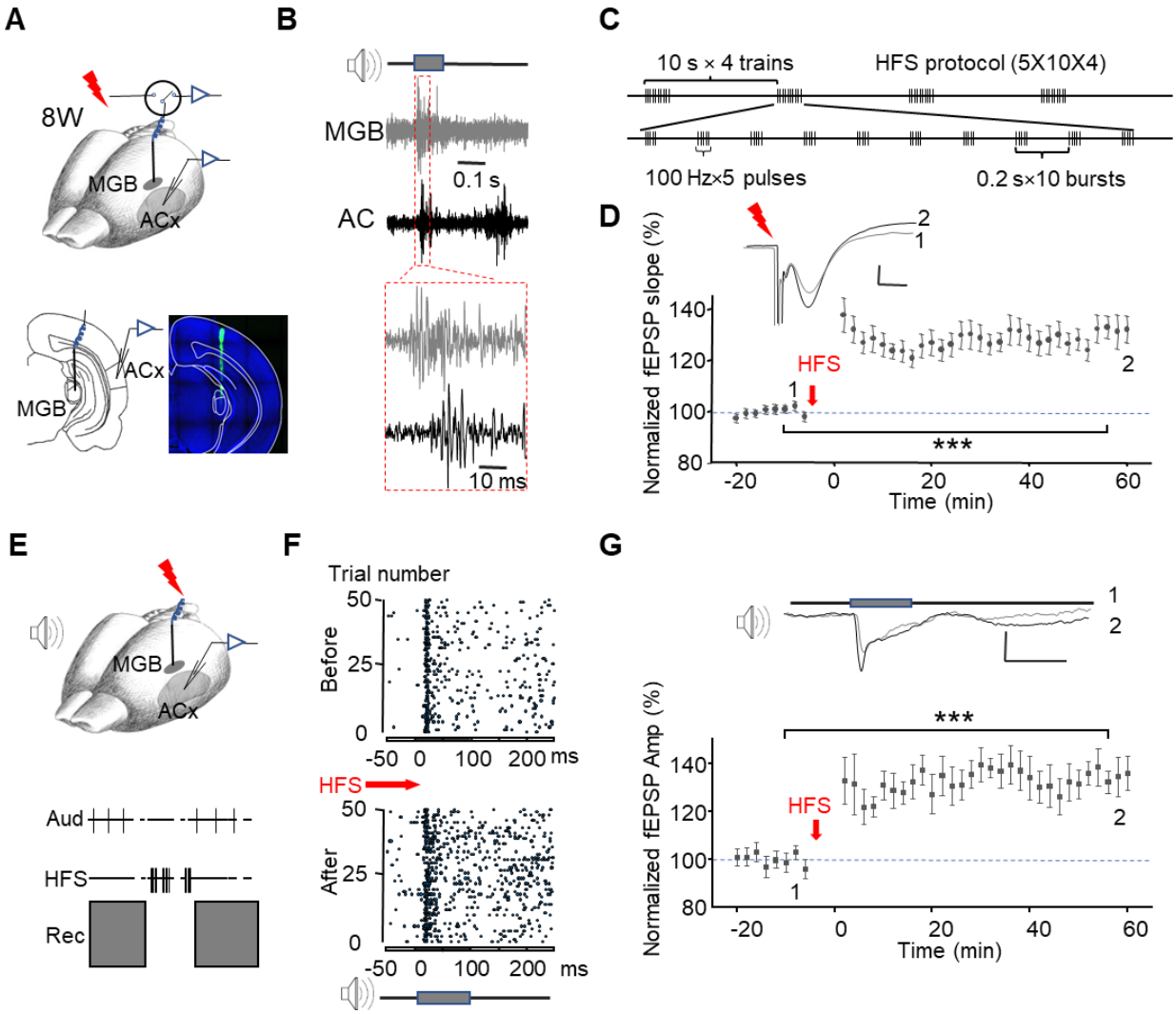

Figure 1. HFS of the MGB induces thalamocortical LTP in the ACx.

(A) Experimental setup. The stimulation electrode array (ES) was inserted into the MGB, while the recording electrode array was placed into the ACx.

(B) Raw extracellular multiunit recording signals form the MGB and the ACx are shown. Noise bursts of 100 ms duration and 70dB intensity were presented during electrode insertion. Robust

auditory responses were recorded when the electrodes reached layer IV of the ACx and the ventral division of MGB, respectively.

(C) HFS protocol. Each burst includes five 0.5-ms pulses at 100 Hz, and each block consists of 10 bursts at 5 Hz. Four blocks were delivered with an inter-block interval of 10 s.

(D) HFS-induced LTP in the auditory thalamocortical pathway. Upper: Sample fEPSP waveforms evoked by ES in MGB before (Gray, 1) and after (Black, 2) HFS in MGB. Scale bar: 10 ms, 0.1 mV. Lower: Population data of normalized fEPSP slopes recorded in ACx before and after HFS (n = 13 from 10 young adult mice, One-way RM ANOVA, ***, $p < 0.001$).

(E) The preparation (upper) and the paradigm (lower) illustrate the induction of LTP in natural auditory responses.

(F) Raster displays of auditory responses in ACx were compared before and after the thalamocortical LTP induction.

(G) HFS-induced thalamocortical LTP of auditory responses. Upper: Sample fEPSP waveforms evoked by noise bursts before (Gray, 1) and after (Black, 2) HFS in MGB. Scale bar: 0.1 s, 0.2 mV. Lower: Population data of normalized fEPSP amplitude recorded in the ACx before and after HFS (n=17 from 6 mice, One-way RM ANOVA, ***, $p < 0.001$).

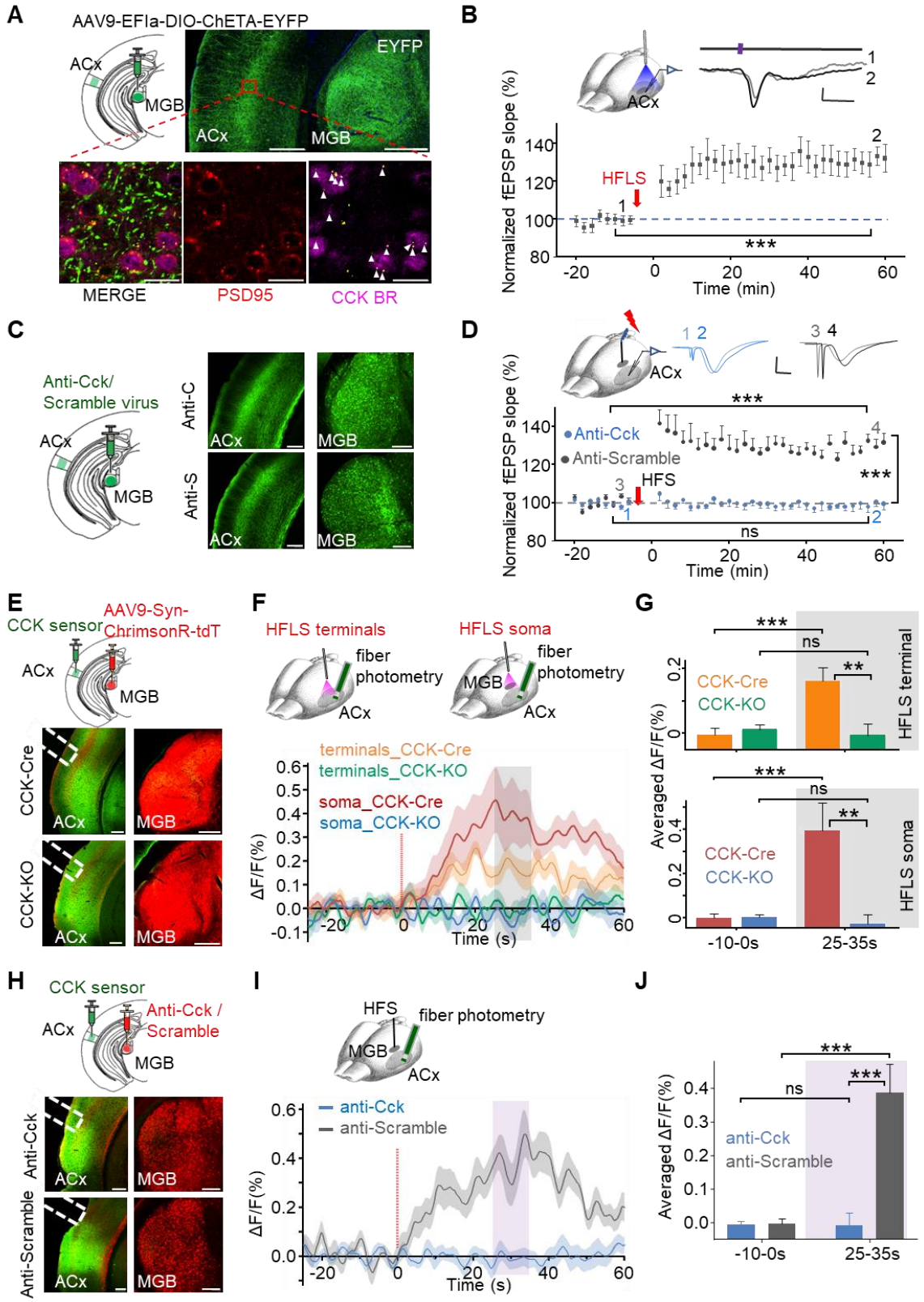
A
AAV9-EF1a-DIO-ChETA-EYFP
ACx
MGB
EYFP
MERGE
PSD95
CCK BR
B
Normalized fEPSP slope (%)
HFLS
Time (min)
C
Anti-Cck/
Scramble virus
Anti-C
Anti-S
D
Anti-Cck
Anti-Scramble
HFS
ns
E
CCK sensor
AAV9-Syn-
ChrimsonR-tdT
CCK-Cre
CCK-KO
F
HFLS terminals
HFLS soma
fiber
photometry
terminals_CCK-Cre
terminals_CCK-KO
soma_CCK-Cre
soma_CCK-KO
ΔF/F(%)
Time (s)
G
Averaged ΔF/F(%)
HFLS terminal
HFLS soma
-10-0s
25-35s
H
Anti-Cck /
Scramble
Anti-Cck
Anti-Scramble
I
anti-Cck
anti-Scramble
J

1004

Figure 2. Thalamocortical LTP is CCK-dependent.

(A) The Cre-dependent virus-infected CCK-positive thalamocortical projection neurons in CCK-Cre mice. Histological confirmation of the virus expression in the ACx and MGB (Green: EYFP). The post-synaptic marker PSD95 was labeled in red. Lower right: CCK-B receptors are labeled by far-red-fluorescent dye and represented in magenta. Thalamocortical terminals (Yellow dots) and their co-localization with CCKBR are indicated by white arrowheads. Scale bar: Upper, 300 µm; Lower, 20 µm.

(B) Induction of LTP in the thalamocortical pathway by high-frequency laser stimulation (HFLS) of CCK-positive thalamocortical fibers in the ACx. Upper left: Experiment design diagram. Upper right: Representative waveforms of laser-evoked fEPSPs before (Gray, 1) and after (Black, 2) the HFLS. Scale bar: 40 ms, 20 µV. Lower panel: Normalized slopes of laser-evoked fEPSPs for 16 mins before and 1h after HFLS in the ACx (n=25 from 5 mice, one-way ANOVA, ***, $p < 0.001$).

(C) Left panel: Schematic diagram illustrating the injection of mice with AAV expressing short hairpin RNA (shRNA) targeting Cck (anti-Cck: rAAV-hSyn-EGFP-5'miR-30a-shRNA(Cck)-3'-miR30a-WPREs) or a scrambled sequence (anti-Scramble: rAAV-hSyn-EGFP-5'miR-30a-shRNA(Scramble)-3'-miR30a-WPREs). Right panel: Post-hoc verification of viral expression in the MGB area and thalamocortical projections distributed in the ACx area (scale bars: 200 µm).

(D) Upper left: Experiment design diagram. Upper right: Representative traces of the evoked fEPSP before (1,3) and after (2,4) HFS in the two groups. Anti-Scramble is indicated in gray,

and anti-Cck is indicated in blue. Scale bar: 10 ms, 0.1 mV. Lower panel: Normalized fEPSP slope before and after HFS in mice expressing anti-Cck (Blue, ns, $p = 0.859$, $n = 16$ from 10 mice) or anti-Scramble (Gray, ***, $p < 0.001$, $n = 17$ from 8 mice) shRNA (Anti-Cck vs. Anti-Scramble after HFS, two-way ANOVA, ***, $p < 0.001$).

(E) AAV9-syn-CCKsensor was injected into ACx, and AAV9-Syn-FLEX-ChrimsonR-tdTomato/AAV9-Syn-ChrimsonR-tdTomato was injected into the MGB of CCK-ires-Cre/CCK-KO mice. Enlarged images show the expression of AAV9-hSyn-Chrimson-tdTomato in the MGB (upper right) and thalamocortical projections with CCK-sensor expression (scale bars: 200 μm).

(F) Upper: Experiment design diagram. An optical fiber was attached to the surface of ACx to activate thalamocortical terminals (left) or inserted into the MGB to activate the cell body (right). Another optical fiber was placed in the ACx to monitor fluorescence intensity. Lower: Traces of fluorescence signals of the CCK-sensor before and after HFLS (red light) in CCK-Cre or CCK-KO mice. The averaged $\Delta F/F0\%$ is shown as the mean value in solid line with the SEM represented by the shadow area. Fluorescence increased after HFLS in CCK-Cre mice (Orange, terminal activation; red, soma activation), but HFLS failed to induce an increase in CCK-KO mice (green, terminal activation; blue, soma activation).

(G) Bar charts present the averaged $\Delta F/F0\%$ from different groups before and after HFLS (Bonferroni multiple comparisons adjustment: Upper, before vs. after HFLS at terminal in CCK-Cre: ***, $p < 0.001$, $n = 16$, $N = 8$; before vs. after HFLS at terminal in CCK-KO: ns, $p = 0.616$, $n = 14$, $N = 7$; After HFLS at terminal in CCK-Cre vs. CCK-KO: **, $p = 0.004$; Lower, before

vs. after HFLS at soma in CCK-Cre: ***, $p < 0.001$, $n = 21$, $N = 11$; before vs. after HFLS at soma in CCK-KO: ns, $p = 0.723$, $n = 20$, $N = 10$; After HFLS at soma in CCK-Cre vs. CCK-KO: **, $p = 0.003$).

(H) AAV9-syn-CCK sensor was injected into ACx, and anti-CCK (rAAV-hSyn-mCherry-5'miR-30a-shRNA(Cck)-3'-miR30a-WPREs) /anti-Scramble (rAAV-hSyn-mCherry-5'miR-30a-shRNA(Scarmble)-3'-miR30a-WPREs) shRNAs were injected into the MGB of C57 mice. Enlarged images show the expression of shRNAs in the MGB (lower right) and thalamocortical projections with CCK sensor (lower left) expression (scale bars: 200 μm).

(I) Upper: Experiment design diagram. A stimulation electrode was inserted into MGB for HFS. Another optical fiber was placed in ACx to monitor the fluorescence intensity. Lower: Traces of fluorescence signal of the CCK-sensor before and after the HFS in the anti-Cck group or anti-Scramble group. The Averaged $\Delta F/F0\%$ is shown as the mean value in solid line with the SEM represented by the shadow area. Fluorescence increased after HFS of MGB in the anti-Scramble group (gray), but the HFS failed to induce an increase in the anti-Cck group (blue).

(J) Bar charts present the averaged $\Delta F/F0\%$ from different groups before and after HFS (Bonferroni multiple comparisons adjustment: before vs. after HFS in anti-Scramble group: ***, $p < 0.001$, $n = 21$ from 11 mice; before vs. after HFS in anti-Cck group: ns, $p = 0.999$, $n = 22$ from 11 mice; After HFLS in anti-Scramble group vs. anti-Cck group: ***, $p < 0.001$).

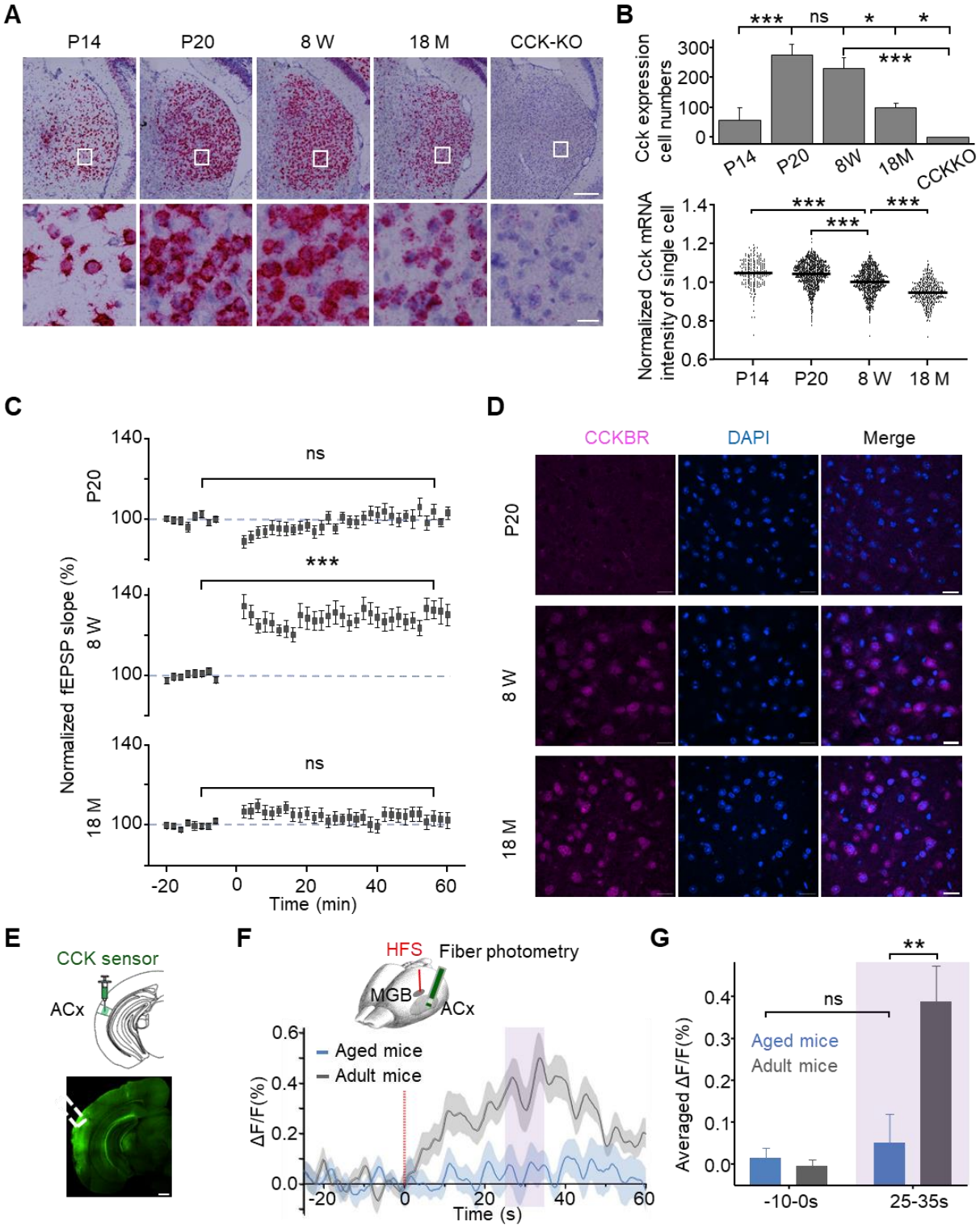
A
P14
P20
8 W
18 M
CCK-KO
B
Cck expression cell numbers
300
200
100
0
***
ns
*
*
***
P14
P20
8W
18M
CCKKO
Normalized Cck mRNA intensity of single cell
1.4
1.2
1.0
0.8
0.6
***
***
***
P14
P20
8 W
18 M
C
Normalized fEPSP slope (%)
P20
8 W
18 M
140
100
ns
***
ns
-20
0
20
40
60
Time (min)
D
CCKBR
DAPI
Merge
P20
8 W
18 M
E
CCK sensor
ACx
F
HFS
Fiber photometry
MGB
ACx
Aged mice
Adult mice
ΔF/F(%)
0.6
0.4
0.2
0.0
-20
0
20
40
60
Time (s)
G
Averaged ΔF/F(%)
0.4
0.3
0.2
0.1
0.0
ns
**
Aged mice
Adult mice
-10-0s
25-35s

1066

Figure 3. Cholecystokinin correlates with developmental thalamocortical LTP in the MGB

(A) Expression of Cck mRNA in MGB of different age groups and CCK-KO mice. Scale bar: Upper, 200 µm; Lower, 20 µm.

(B) Comparison of Cck expression level in different age groups and CCK-KO mice. Upper panel: The number of Cck-expression cells in MGv (see Methods) for each group (One-way ANOVA, Bonferroni multiple comparisons adjustment: P14 vs. P20, ***, $p < 0.001$; P20 vs. 8W, ns, $p = 1.0$; 8W vs. 18M, *, $p = 0.018$; 18M vs. CCK-KO, *, $p = 0.05$; 8W vs. CCK-KO, ***, $p < 0.001$. n of P14 = 4 from 2 mice; n of P20 = 4 from 2 mice; n of 8W = 4 from 2 mice; n of 18M = 4 from 2 mice; n of CCK-KO = 8 from 4 mice). Lower panel: Normalized CCK mRNA intensity of single cells (see Methods) in different age groups (One-way ANOVA, Bonferroni multiple comparisons adjustment: P14 vs. 8W, ***, $P < 0.001$; P20 vs. 8W, ***, $P < 0.001$; 8W vs. 18M, ***, $P < 0.001$; n of P14 = 228 neurons; n of P20 = 1104 neurons; n of 8W = 929 neurons; n of 18M = 400 neurons).

(C) HFS-induced thalamocortical LTP at different developmental stages. Normalized fEPSP slopes before and after HFS in the MGB at P20, 8W, and 18M (P20, upper, ns, $p = 0.542$, n=15 from 10 mice; 8W, middle, ***, $p < 0.001$, n = 13 from 10 mice; 18M, lower, ns, $p = 0.380$, n = 18 from 8 mice).

(D) Expression of CCKBR in ACx neurons at different ages. Immunostained CCKBR expression in the ACx neurons at P20, 8W and 18M. CCK: red; DAPI: blue. Scale bar: 20 µm.

(E) Injection of AAV9-syn-CCK sensor into ACx of aged mice (18M). Enlarged images displaying the CCK-sensor expression in the ACx (Scale bar: 500 μm).

(F) Upper: Experiment design diagram. A stimulation electrode was inserted into MGB to apply HFS, and an optical fiber was placed in the ACx to monitor fluorescence intensity. Lower: Traces of fluorescence signal of the CCK-sensor before and after HFS in aged mice (blue). The fluorescence signals from anti-Scramble group (gray) in Figure 2I were utilized as adult control (3 ~ 4 M). The averaged ΔF/F0% is shown as the mean value in solid line with the shadow area indicating the SEM. HFS failed to induce an increase in fluorescence in aged mice.

(G) Bar charts showing the averaged ΔF/F0% from the different groups before and after HFS (Statistical analysis with Bonferroni multiple comparisons adjustment: before vs. after HFS in aged mice: ns, $p = 0.699$, $n = 12$ from 6 mice; after HFS in aged mice vs. adult control group: **, $p = 0.01$).

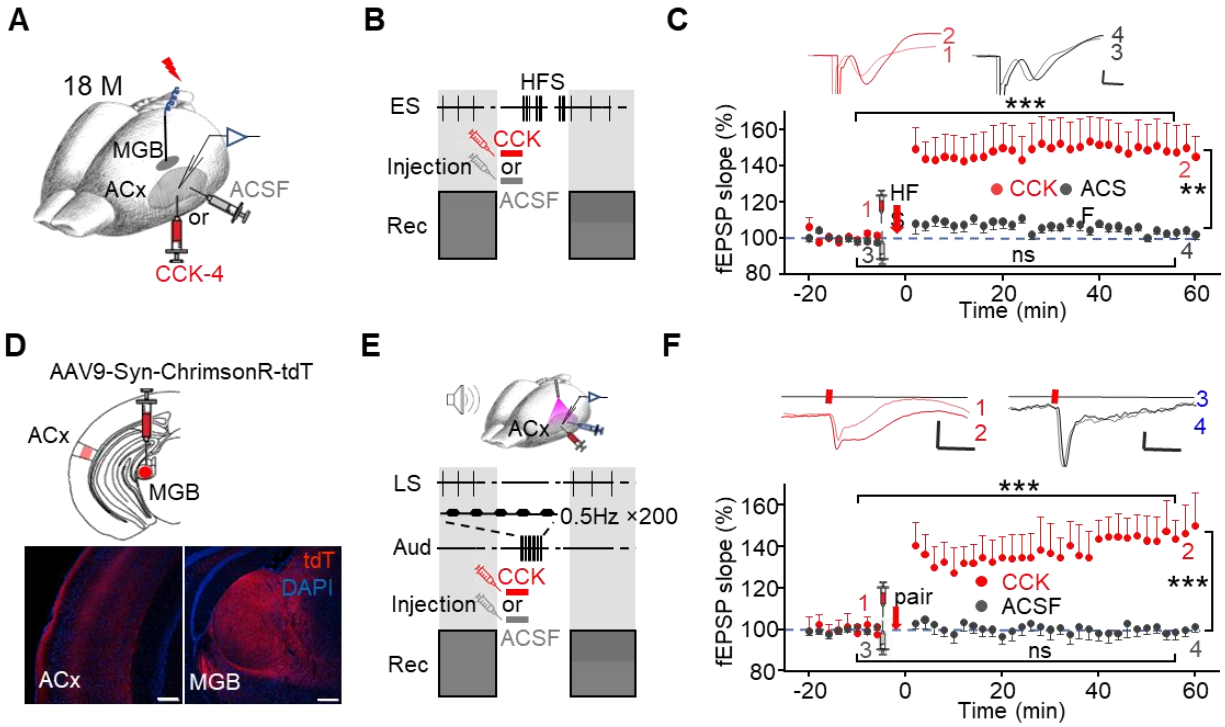

Figure 4. Exogenous application of CCK rescues thalamocortical connectivity.

(A) Experiment design diagram illustrating the electrode and drug-injection pipette placement.

(B) Experimental protocol. CCK or ACSF was injected into the ACx, followed by HFS in the MGB. The fEPSPs in response to MGB ES were recorded before and after the intervention.

(C) CCK-4 injection rescued the HFS-induction of thalamocortical LTP in aged mice. Upper: Representative traces of the evoked fEPSP before (1,3) and after (2,4) injection followed by HFS in the CCK-4 (red) and ACSF group (gray). Scale bar: 10 ms, 0.1 mV. Lower panel: Normalized fEPSP slope before and after CCK-4 (red) or ACSF (gray) injection in the ACx followed by HFS in the MGB of the old mice (CCK-4: n = 13 from 6 mice, ***, $p < 0.001$; ACSF: n = 12 from 7 mice, ns, p = 0,404; CCK vs. ACSF after the intervention, **, p = 0.006).

(D) Upper: AAV9-hSyn-ChrimsonR-tdTomato was injected into the MGB of C57 mice. Lower panel: Histological confirmation of virus expression in both the ACx and the MGB (Scale bars: 100 μm).

(E) Upper panel: Experiment design diagram. A laser with a wavelength of 620-nm was used to activate thalamocortical terminals expressing opsins in the ACx. Glass pipette electrodes in the ACx recorded the field EPSPs evoked by laser stimulation. Lower panel: Experimental protocol. CCK or ACSF was injected into the ACx, followed by 200 auditory stimulations. fEPSPs in response to laser stimulation were recorded before and after the intervention.

(F) Upper: Representative fEPSP traces evoked by laser before (1,3) and after (2,4) the intervention in different groups. Scale bars: left, 40 ms, 0.1 mV; right, 40 ms, 20 μV. Lower: Normalized slopes of laser-evoked fEPSPs for 16 mins before and 1h after injection followed by auditory stimulation (two-way RM ANOVA, before vs. after: CCK group, ***, $p < 0.001$, $n = 10$ from 10 mice; ACSF group, ns, $p = 0.899$, $n = 19$ from 10 mice; CCK vs. ACSF after the intervention, $p < 0.001$).

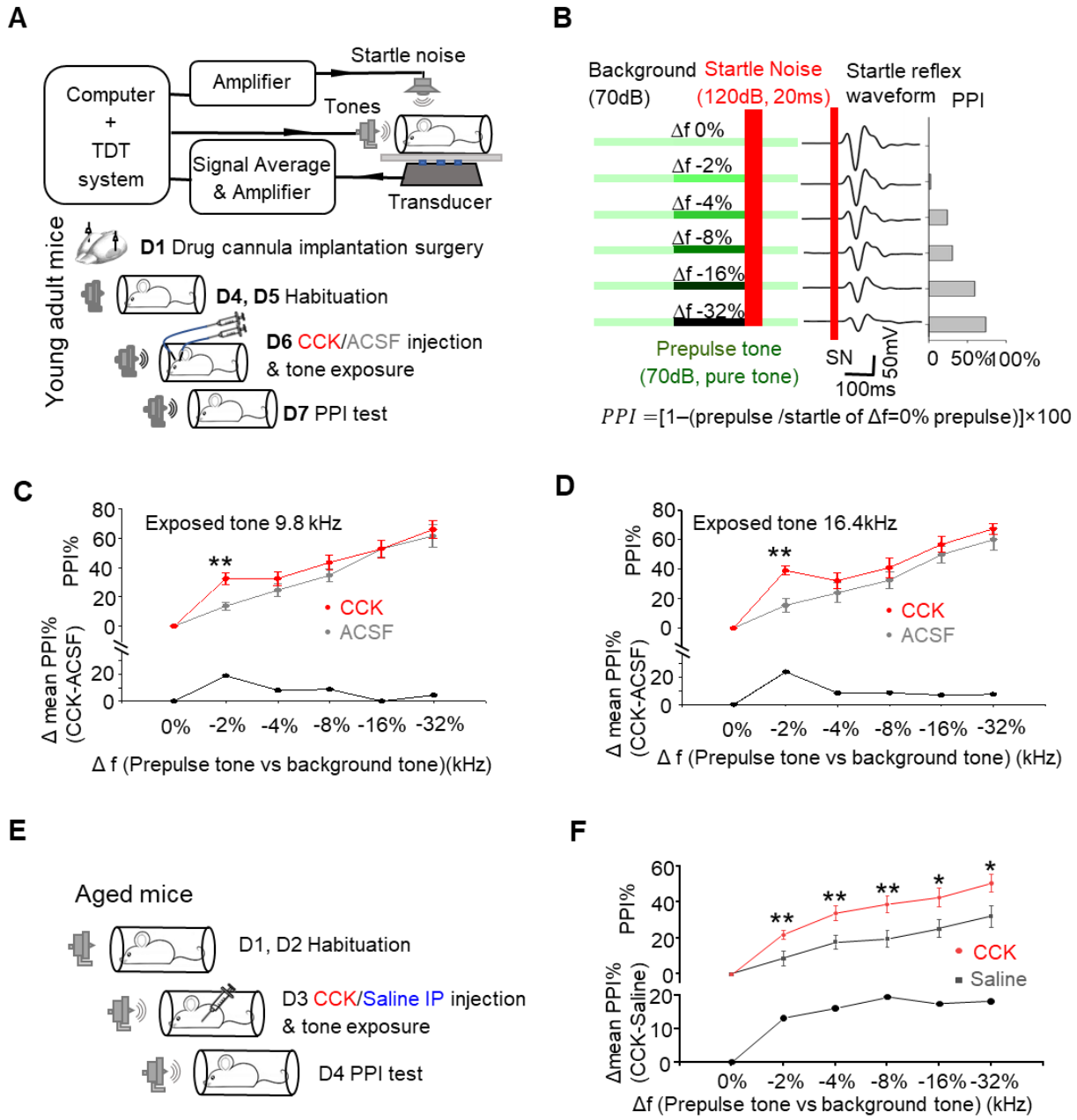

Figure 5. Exogenous application of CCK enhances frequency discrimination.

(A) Upper: Schematic diagram of the experimental behavior setup. lower: Experimental procedures of passive tone exposure with CCK/ACSF injection into the ACx of young adult mice.

(B) Left: Prepulse inhibition acoustic startle test protocol: a continuous background pure tone at 70 dB (9.8 kHz or 16.4 kHz), was presented during the test, except when the prepulse tones and startle noises were delivered. Prepulse inhibition trials were presented in a pseudorandom order. Each prepulse test consisted of an 80 ms prepulse at 70dB (Δf, pure-tone frequency was 0%, 2%, 4%, 8%, 16%, or 32% lower than the background tone), followed by a 20 ms white noise startle pulse at 120 dB, and then the background tone resumed after the startle. Each test was repeated 15 times. Middle: examples of averaged startle waveforms from a sampled mouse. Right: Prepulse inhibition (PPI as defined below) for the examples.

(C) Mean PPI (%) of the startle responses in C57 mice exposed to 9.8 kHz tone after CCK-8S (red line) or ACSF (gray line) injection into the ACx (CCK, n=7, ACSF n=7, two-way ANOVA, $p<0.05$, post-hoc, Tukey test, CCK vs. ACSF in $\Delta f = -2\%$, **, $p<0.001$). Prepulse frequencies were 0, 2, 4, 8, 16, or 32% lower than the background tone, 9.8 kHz. The difference in the mean PPI between the CCK infusion and ACSF infusion groups is listed as a function of the Δf below.

(D**)** Mean PPI of startle responses in C57 mice exposed to a 16.4 kHz tone after CCK-8S (red line) or ACSF (gray line) injection into the ACx (CCK n=8, ACSF n=7, two-way ANOVA, $p<0.05$, post-hoc, Tukey test, CCK vs. ACSF in $\Delta f = -2\%$, **, $p<0.001$). Prepulse frequencies were 0, 2, 4, 8, 16, or 32% lower than the background tone, 16.4 kHz. The difference in the mean PPI between the CCK infusion and ACSF infusion groups is listed as a function of the Δf below.

(E) Experimental procedures of passive tone exposure with CCK/Saline I.P. injection in aged mice.

(F) Mean PPI of startle responses in aged mice exposed to a 9.8 kHz tone after i.p. injection of CCK-4 (red) or Saline (gray). Prepulse frequencies were 0, 2, 4, 8, 16, or 32% lower than background tone, 9.8 kHz. The difference in mean PPI between the CCK-4 injection and Saline injection groups is listed as a function of the Δf below (Bonferroni-adjusted multiple comparisons with CCK vs. Saline in Δf =: **-2%**, **, p = 0.010; **-4%**, **, p = 0.006; **-8%**, **, p = 0.006; **-16%**, *, p = 0.022; **-32%**, *, p = 0.027; Frequency-discrimination task in CCK-4 group vs. Saline group, two-way ANOVA, **, p = 0.004; CCK-4, N = 15; Saline, N = 15).

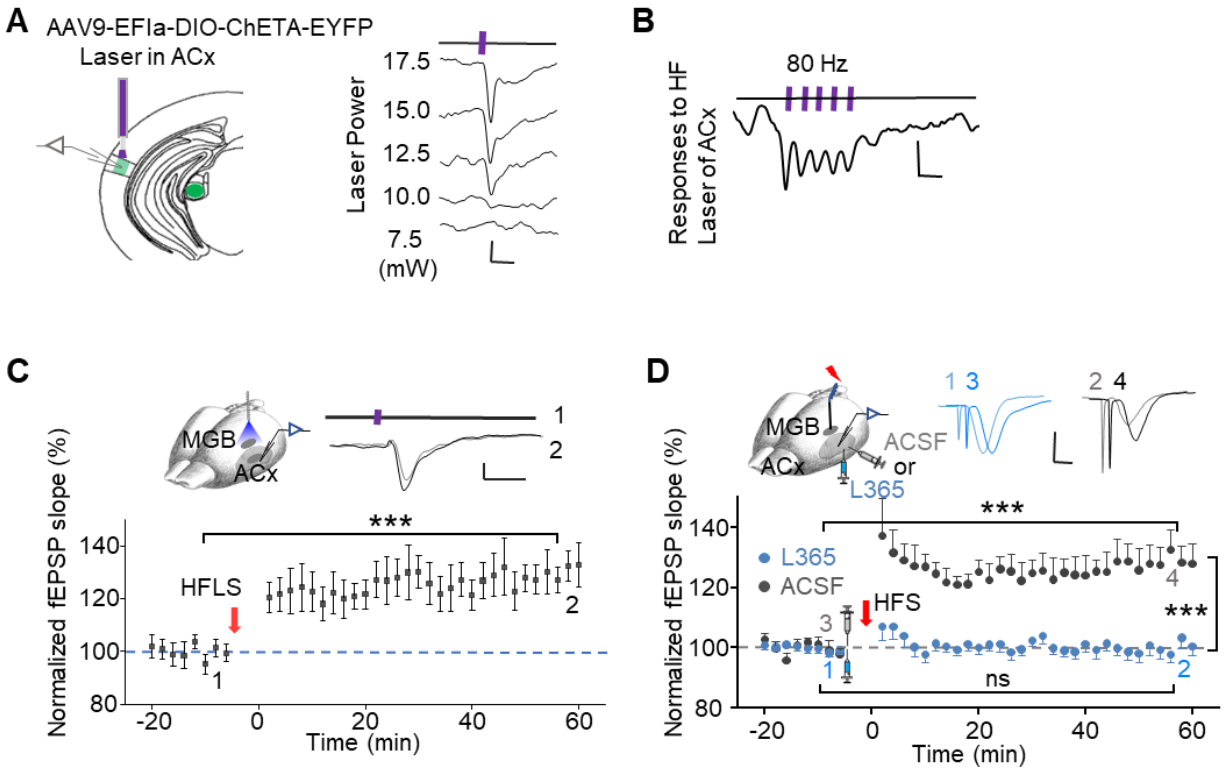

Figure S1. Thalamocortical LTP is CCK-dependent, related to Figure 2.

(A) Neuronal responses in field potentials evoked by laser stimulation of CCK-positive thalamocortical fibers in the ACx. Left, Schematic showing the position of laser fiber in the ACx. Right, evoked fEPSPs increased with higher laser power. Scale bar: 20 ms, 20 µV.

(B) fEPSPs elicited by the high-frequency (HF) laser pulse train demonstrated that fEPSPs in the ACx could follow the laser stimulation with 80Hz. Scale bar: 20 ms, 20 µV.

(C) HF laser stimulation (HFLS) of CCK-positive neurons in the MGB induced LTP in the thalamocortical pathway. Upper left: Experiment design diagram. Upper right: Sample laser-evoked fEPSP waveforms before (Gray, 1) and after (Black, 2) HFLS. Scale bar: 50 ms, 20 µV.

Lower panel: Normalized slopes of laser-evoked fEPSPs for 16 mins before and 1h after HFLS in the MGB (one-way ANOVA, ***, $p<0.001$, n=18 from 6 mice).

(D) CCKBR antagonist blocked HFS-induced thalamocortical LTP. Upper left: Experiment design diagram. Upper right: Representative traces of the evoked fEPSP before (1,3) and after (2,4) induction in the two groups. ACSF group is indicated in gray, and L365 group is indicated in blue. Scale bar: 10 ms, 0.1 mV. Lower panel: Normalized fEPSP slope before and after drug application followed by HFS in the MGB (L365 group, blue, ns, $p = 0.779$, n = 22 from 5 mice; ACSF group, gray, ***, $p < 0.001$, n = 12 from 5 mice).

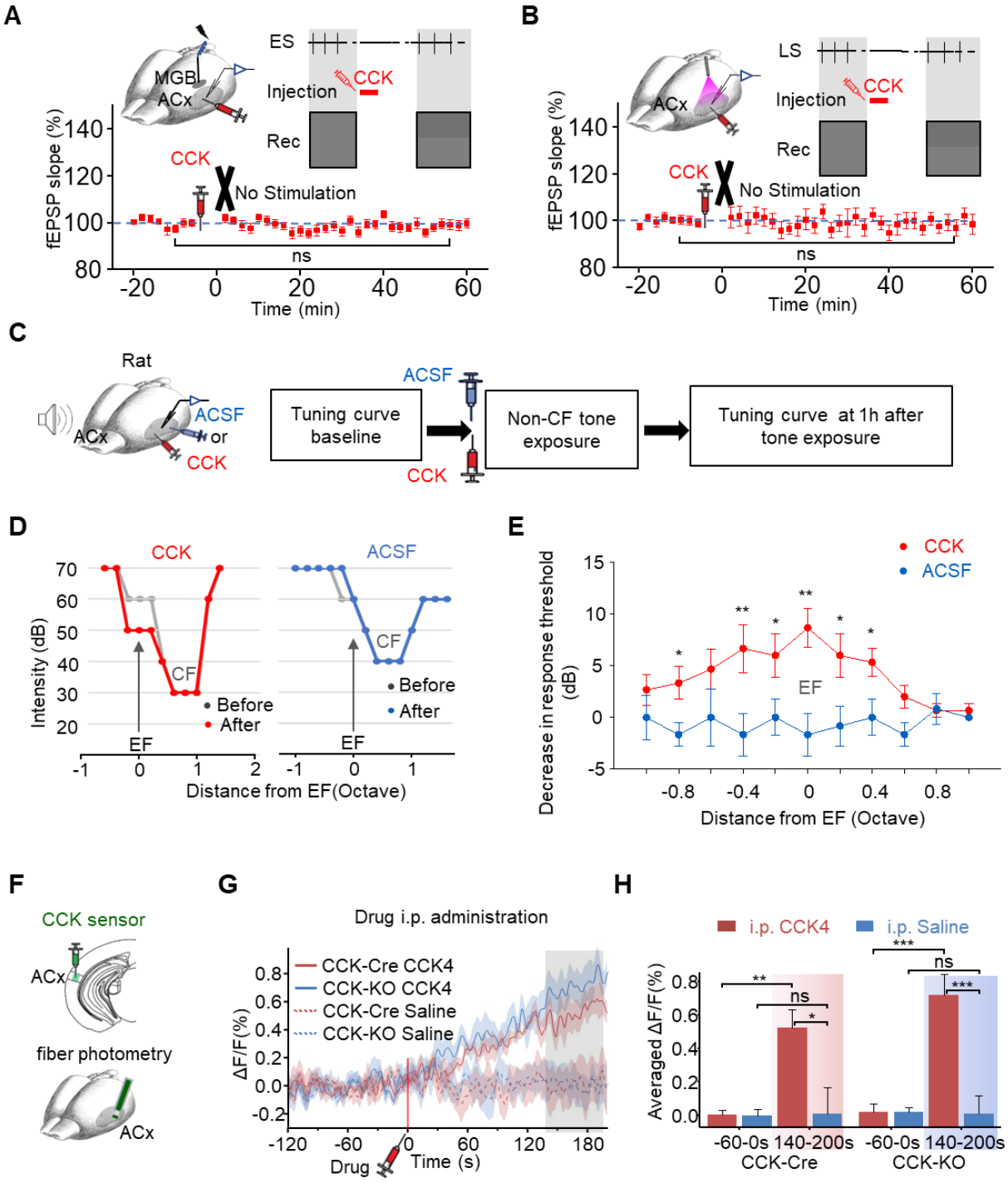

Figure S2. Exogenous application of CCK rescued thalamocortical LTP in aged mice and enhanced frequency discrimination ability, related to Figure 4 and Figure 5.

(A) Upper left: Experiment design diagram showing electrodes and drug-injection pipette placement. Upper right: Experimental protocol. CCK was injected into the ACx without stimulation. Lower: Normalized fEPSP slope in response to ES before and after CCK-4 injection in the ACx (one-way RM ANOVA, ns, $p = 0.956$, $n = 20$ from 5 mice).

(B) Upper left: Experiment design diagram showing electrodes, optical fiber, and drug-injection pipette placement. Upper right: the Experimental protocol. CCK was injected into the ACx without stimulation. Lower: Normalized fEPSP slope in response to laser before and after CCK-4 injection in the ACx (one-way RM ANOVA, ns, $p = 0.468$, $n = 22$ from 4 mice).

(C) Left: Schematic drawing of the experiment setup. Right: Experimental paradigm.

(D) Left: Sample tuning curves before (gray line) and after (red line) CCK-8S infusion and a non-CF tone exposure. The arrow above the horizontal axis indicates the exposed frequency (EF). Right: Sample tuning curves before (gray line) and after (blue line) ACSF infusion and a non-CF tone exposure. The arrow above the horizontal axis indicates the exposed frequency (EF).

(E) Population data showing the changes in responding thresholds after CCK-8S (red line) or ACSF (blue line) infusion followed by tone exposure (CCK-8S, n=15; ACSF n=12, two-way ANOVA, $p<0.001$, post-hoc, Tukey test, CCK-8S vs. ACSF, *$p<0.05$, **$p<0.001$).

(F) Left: Experiment design diagram showing the placement of an optical fiber in the ACx for monitoring the fluorescence intensity.

(G) Traces of fluorescence signal of the CCK-sensor before and after the CCK-4 (1 mg/kg) or saline i.p. injection in CCK-Cre mice or CCK-KO mice. Averaged $\Delta F/F0\%$ is shown as the

mean value in solid line and SEM in the shadow area. The fluorescence increased after CCK-4 application (solid) in both CCK-Cre mice (red) and CCK-KO mice (blue), while saline application (dashed) did not induce an increase.

(H): Bar charts showing the averaged ΔF/F0% from the different groups before and after drug application. (Left panel: Averaged ΔF/F0% of CCK-Cre mice, two-way ANOVA followed by Bonferroni multiple comparisons adjustment, before vs. after CCK-4 treatment: red, **, $p = 0.002$, N = 7; before vs. after saline treatment: blue, ns, $p = 0.951$, N = 9; After CCK-4 vs. after Saline: *, $p = 0.025$; Right panel: Averaged ΔF/F0% of CCK-KO mice, two-way ANOVA followed by Bonferroni multiple comparisons adjustment, before vs. after CCK-4 treatment: red, ***, $p < 0.001$, N=7; before vs. after saline treatment: blue, ns, $p = 0.877$, N = 8; After CCK-4 vs. after Saline: ***, $p = 0.001$).